

Grand Design vs. Multi-Armed Spiral Galaxies: Dependence on Galaxy Structure

BEVERLY J. SMITH,¹ MATTHEW WATSON,¹ MARK L. GIROUX,¹ AND CURTIS STRUCK²

¹*East Tennessee State University
Department of Physics and Astronomy, Box 70652
Johnson City TN 37614, USA*

²*Iowa State University
Department of Physics and Astronomy
Ames IA 50011, USA*

ABSTRACT

We developed an algorithm to use Galaxy Zoo 3D spiral arm masks produced by citizen scientist volunteers to semi-automatically classify spiral galaxies as either multi-armed or grand design spirals. Our final sample consists of 299 multi-armed and 245 grand design galaxies. On average, the grand design galaxies have smaller stellar masses than the multi-armed galaxies. For a given stellar mass, the grand design galaxies have larger concentrations, earlier Hubble types, smaller half-light radii, and larger central surface mass densities than the multi-armed galaxies. Lower mass galaxies of both arm classes have later Hubble types and lower concentrations than higher mass galaxies. In our sample, a higher fraction of grand design galaxies have classical bulges rather than pseudo-bulges, compared to multi-armed galaxies. These results are consistent with theoretical models and simulations which suggest that dense classical bulges support the development and/or longevity of 2-armed spiral patterns. Similar specific star formation rates are found in multi-armed and grand design galaxies with similar stellar masses and concentrations. This implies that the specific star formation rates in spiral galaxies is a function of concentration and stellar mass, but independent of the number of spiral arms. Our classifications are consistent with arm counts from the Galaxy Zoo 2 project and published $m=3$ Fourier amplitudes.

Keywords: Disk Galaxies — Spiral Galaxies — Galaxy Evolution

1. INTRODUCTION

Galaxy morphological classification as introduced by Hubble (1926) divides spiral galaxies into Hubble types based upon the bulge-to-disk ratio, the tightness of the spiral arms, and the ‘degree of resolution in the arms’. An alternative method of classifying spiral galaxies based upon the number and appearance of the spiral arms was introduced by the Elmegreens in a series of papers (Elmegreen 1981; Elmegreen & Elmegreen 1982, 1984, 1987; Elmegreen et al. 2011). In the modern version of the Elmegreen arm class system, grand design galaxies have two long continuous spiral arms, flocculent galaxies have multiple short fragments of spiral arms, and galaxies with three or more moderately long arms are classified as multi-armed (Elmegreen et al. 2011; Buta et al. 2015). Applying both classification schemes in parallel and examining galactic properties such as stellar mass (M^*), concentration, bulge structure, star formation rate (SFR), and specific SFR (sSFR) may provide clues to the mechanisms that excite and maintain spiral arms in galaxies.

Several processes may generate spiral arms in galaxies, including interactions between galaxies, central bars, and gravitational instabilities in differentially rotating disks. In classical spiral density wave theory, waves with fixed pattern speeds travel through the disk (Lin & Shu 1964, 1966). Without some means of rejuvenation, however, spiral waves will disperse within a few galactic revolutions (Toomre 1969). In theory, a large bulge may stabilize a spiral density wave. Galaxies with large bulges are expected to have high Toomre Q parameters in their centers, and a high Q may reflect incoming waves, producing a 2-armed standing wave that is long-lived (Lin & Bertin 1985; Bertin et al. 1989). Whether stable wave modes like these occur in real galaxies is uncertain. Sellwood (2011) found only transient spiral patterns in a set of simulations based on the Bertin et al. (1989) scenario, but more recent simulations by Saha & Elmegreen (2016) produced long-lived two-armed spiral patterns with constant pattern speeds.

Spiral arms may also be caused by gravitational instabilities in a differentially rotating disk (Goldreich & Lynden-Bell 1965; Julian & Toomre 1966; Sellwood 2012; Baba et al. 2013). In this scenario, the spiral is enhanced by the galactic shear in a process called swing amplification (Julian & Toomre 1966; Toomre 1981; Baba et al. 2013; D’Onghia et al. 2013; Michikoshi & Kokubo 2018; Dobbs & Baba 2014). Such arms may be self-perpetuating and therefore long-lived in a statistical sense (D’Onghia et al. 2013). Whether the arms are fragmented or continuous may depend upon the relative amount of stellar feedback; higher feedback tends to produce a more flocculent structure in these models (Dobbs et al. 2018). Spiral structure may persist longer in disks with on-going star formation because of dynamical cooling (Sellwood & Carlberg 1984).

Grand design spirals may also be driven by galactic bars (Sanders & Huntley 1976; Kormendy & Norman 1979; Athanassoula 1980). Alternatively, a gravitational perturbation by a neighboring galaxy can induce a 2-armed spiral pattern according to models (Toomre & Toomre 1972; Byrd & Howard 1992; Dobbs et al. 2010; Struck et al. 2011). In addition to M51-like interactions between galaxies in bound pairs (Dobbs et al. 2010), rapid flyby encounters may also induce spiral arms that can be long-lived (Oh et al. 2008; Struck et al. 2011).

The role of each of these mechanisms in creating the observed spiral patterns of galaxies remains controversial (see recent reviews by Dobbs & Baba (2014), Shu (2016), and Sellwood & Masters (2022)). To distinguish between these scenarios, observational studies in which the number of arms and/or the arm class is compared with various properties of the galaxies are helpful.

Past studies show some limited correlation between Hubble type and arm class. Flocculent galaxies tend to have later Hubble types than grand design galaxies, but there is considerable variation among the Hubble types of galaxies in a given arm class (Elmegreen & Elmegreen 1982; Ann & Lee 2013; Bittner et al. 2017; Díaz-García et al. 2019). Galaxies with grand design patterns are more likely to have large bulges (Bittner et al. 2017). Flocculent galaxies tend to be smaller than grand design galaxies (Elmegreen & Elmegreen 1987) and have lower stellar masses (Bittner et al. 2017).

To test spiral arm models observationally, large samples of galaxies with quantitative estimates of the number of arms are needed. One way to efficiently extract quantitative measures of spiral arm properties for a large number of galaxies is via Fourier analysis. The largest such study done to date is that of Yu & Ho (2020), who studied 4378 face-on (ellipticity ≤ 0.5) Sloan Digital Sky Survey (SDSS) disk galaxies with $z \leq 0.05$. Using 1-dimensional and 2-dimensional Fourier decomposition of the SDSS r images, Yu & Ho (2020) derived an average arm strength and an average spiral arm pitch angle for each galaxy. They also calculated a parameter known as f_3 , which is the radially-averaged ratio of the $m=3$ Fourier component amplitude to the sum of the $m=2$, $m=3$, and $m=4$ components. The f_3 parameter is an approximate measure of the number of spiral arms (Elmegreen et al. 2011; Yu et al. 2018). Yu & Ho (2020) found that galaxies with larger central concentrations and earlier Hubble types tend to have smaller f_3 parameters, implying fewer arms. In a followup paper comparing the Yu & Ho (2020) dataset to other parameters, Smith et al. (2022a) found that f_3 is weakly positively correlated with sSFR. However, in subsets of the sample with narrow ranges of concentration, this trend disappears. They conclude that the weak f_3 -to-sSFR correlation is an indirect consequence of both quantities being inversely correlated with concentration.

Another way to obtain estimates of the number of spiral arms in large samples of galaxies is via the Galaxy Zoo 2 (GZ2) citizen scientist survey (Willett et al. 2013). In the GZ2 program, participants were asked a series of questions about a set of galaxies, including their best-guess determinations of the number of arms in each galaxy. GZ2 citizen scientist vote fractions for the number of arms in galaxies have been used in several studies with different galaxy samples, in some cases with seemingly contradictory results. For a luminosity-limited and mass-limited set of 6683 GZ2 SDSS galaxies, Hart et al. (2016) found that the fraction of spiral galaxies that are multi-armed increases with stellar mass, and concluded that multi-armed galaxies have bluer optical colors than 2-armed galaxies, a difference they attributed to enhanced SFRs. However, for a different set of SDSS galaxies, Hart et al. (2017) used ultraviolet and mid-infrared photometry to measure SFRs and found little dependence of SFR and sSFR on the GZ2 arm count, although possibly higher dust extinctions in the 2-armed galaxies. The lack of a relation between arm count and sSFR seen by Hart et al. (2017) is consistent with earlier results by Willett et al. (2015), who found that the SFR- M^* relation for SDSS galaxies is independent of GZ2 arm counts. Porter-Temple et al. (2022) revisited this topic in a later Galaxy Zoo 2 project utilizing more sensitive, better resolution Kilo Degree Survey (KiDS) images from the Very Large Telescope rather than SDSS images. For a set of 1689 galaxies, Porter-Temple et al. (2022) concluded that galaxies with three, four or five arms tend to have higher M^* and higher SFRs than galaxies with two arms, but lower sSFRs.

In a second GZ2 project using KiDS images, [Smith et al. \(2022b\)](#) found that the fraction of galaxies with three arms increases as the optical color becomes bluer.

[Sarkar et al. \(2023\)](#) use a convolutional neural network on SDSS images to classify 1354 SDSS galaxies as either grand design or flocculent, omitting potential multi-armed galaxies from the sample. They trained their code using the [Buta et al. \(2015\)](#) by-eye classifications of 90 grand design and 270 flocculent galaxies. [Sarkar et al. \(2023\)](#) found that the flocculent galaxies identified by their neural network code have lower rotational velocities (lower dynamical masses) and later Hubble types than the galaxies classified as grand design.

As discussed above, the relation of the number of arms to other basic galaxian quantities such as M^* , SFR, sSFR, and concentration remains unsettled. This uncertainty impacts the question of how spiral arms form and evolve with time. Since models of spiral production via disk instabilities and swing amplification tend to produce galaxies with flocculent or multi-armed structure ([Baba et al. 2013](#); [D’Onghia et al. 2013](#); [Dobbs et al. 2018](#)), it is sometimes assumed that grand design galaxies are produced by interactions or bars, while gravitational instabilities produce other spirals ([Dobbs & Baba 2014](#)). However, instability models can also produce 2-armed morphologies if the disk/halo mass ratio is high enough ([Sellwood & Carlberg 1984](#); [D’Onghia 2015](#); [Michikoshi & Kokubo 2018](#)). According to both swing amplification theory and numerical simulations, galaxies with disks that are more massive relative to the halo mass tend to have fewer arms ([Carlberg & Freedman 1985](#); [D’Onghia et al. 2013](#); [D’Onghia 2015](#); [Hart et al. 2018](#); [Michikoshi & Kokubo 2018](#)). The number of arms may also depend upon whether the distribution of dark matter in the halo is ‘cuspy’ or ‘flat’ ([Hart et al. 2018](#)) and on the galactic shear rate ([Michikoshi & Kokubo 2018](#)).

Supporting the theory that grand design spirals are produced by interactions, observational studies have found higher proportions of grand design galaxies among binary galaxies and group galaxies compared to field galaxies ([Elmegreen & Elmegreen 1982](#)). Furthermore, clusters have higher proportions of grand design galaxies compared to the field ([Elmegreen et al. 1982](#); [Choi & Ann 2011](#)). Using GZ2, [Hart et al. \(2016\)](#) found increasing fractions of 2-armed galaxies in higher density regions. [Savchenko et al. \(2020\)](#) also concluded that non-isolated galaxies are more likely to be grand design compared to isolated galaxies. In agreement with these studies, [Smith et al. \(2022a\)](#) found lower normalized $m=3$ Fourier components on average for cluster galaxies than for galaxies in the field, implying a higher percentage of 2-armed galaxies in clusters. However, they attributed their result to galaxies in clusters having larger concentrations than field galaxies. When they compared galaxies with the same concentration and the same mass, the distribution of f_3 values are the same in clusters as in the field. They thus concluded that the number of arms in a galaxy is a product of the internal structure of the galaxy and not the environment.

Observational tests of bar-driven spirals are inconclusive so far. Bar strength and arm strength tend to be correlated ([Block et al. 2004](#); [Buta et al. 2005](#); [Yu & Ho 2020](#)), however, this correlation may mean that conditions in a disk that favor bar production also favor strong arms, rather than bars causing the arms ([Salo et al. 2010](#); [Díaz-García et al. 2019](#)). In any case, the presence of grand design spiral arms in galaxies that are both isolated and unbarred highlights the need for other means of spiral arm production.

In contrast with the suggestion by [Dobbs & Baba \(2014\)](#) that grand design patterns are produced by interactions or bars, [Bittner et al. \(2017\)](#) and [Yu & Ho \(2020\)](#) cite the theoretical work of [Bertin et al. \(1989\)](#) on the reflection of waves by large bulges, and conclude that long-lasting wave modes are responsible for the spiral patterns in high concentration grand design galaxies. This disagreement in the literature illustrates the lack of consensus on the primary mechanisms triggering and maintaining spiral arms in galaxies.

In the current paper, we investigate these questions by deriving arm counts for a large sample of galaxies using a different method. We use spiral arm masks from a different Galaxy Zoo citizen science project, the Galaxy Zoo 3D (GZ-3D) project¹ ([Masters et al. 2021](#)), to count the number of arms in a sample of SDSS spiral galaxies. In Section 2, we describe the sample of galaxies, explain the GZ-3D spiral arm masks, and describe the algorithm we use to count the spiral arms. We compare our arm counts with other properties of the galaxies (stellar mass, concentration, Hubble type, central surface mass density, and sSFR) in Section 3. In Section 4, we compare our arm counts with the [Yu & Ho \(2020\)](#) arm parameters and arm counts from the Galaxy Zoo 2 project. The results are discussed in terms of models of spiral arm production and galaxy evolution in Section 5. Conclusions are given in Section 6. In Appendix A, we show GZ-3D masks and SDSS images of example grand design and multi-armed galaxies in our sample. In Appendix B, we discuss possible selection effects and investigate whether these affect our final conclusions.

Throughout this paper, we assume a Hubble constant of $70 \text{ km s}^{-1} \text{ Mpc}^{-1}$.

¹ <https://www.zooniverse.org/projects/klmasters/galaxy-zoo-3d>

2. SAMPLE AND DATA

2.1. Sample

The GZ-3D sample (Masters et al. 2021) consists of 29,831 SDSS galaxies with $z < 0.15$. The GZ-3D galaxies are a subset of the target list for the SDSS-IV Mapping Nearby Galaxies at APO (MaNGA) integral field unit (IFU) survey, which in turn was selected from the NASA Sloan Atlas (NSA) Version 1.0.1 (Wake et al. 2017). The MaNGA target sample (and therefore the GZ-3D sample) is not a complete sample, but instead was selected to produce approximately uniform coverage in $\log M^*$, and have suitable angular sizes for the MaNGA IFU field of view. The ‘Primary’ MaNGA sample (about 50% of the MaNGA sample) includes galaxies covered by the MaNGA IFU field out to $1.5 \times$ the effective radius of the galaxy, while the ‘Secondary’ MaNGA sample are galaxies observed by the MaNGA IFU out to 2.5 effective radii. A third ‘Color-Enhanced’ sample, making up 17% of the targets, includes galaxies under-represented in the NUV – i color vs. absolute i magnitude diagram, such as high mass blue galaxies and low mass red galaxies.

We limit our sample to galaxies with $z < 0.05$, to allow for sufficient resolution to accurately measure the spiral arms. This is approximately the limit at which one can distinguish grand design from multi-armed galaxies in SDSS images, according to simulations of SDSS images by Yu et al. (2018). We also limit our sample to relatively face-on galaxies with ellipticity in the NSA ≤ 0.5 , where ellipticity = $1 - b/a$, and b and a are the semi-minor and semi-major axis of the galaxy, respectively. This gives us an initial sample of 16,655 galaxies with redshifts between 0.01 and 0.05, and a median redshift of 0.030. This corresponds to distances between 43 and 214 Mpc.

We cross-correlated the Yu & Ho (2020) galaxy list with the Masters et al. (2021) Galaxy Zoo-3D sample. A total of 1002 galaxies are in both the GZ-3D and Yu & Ho (2020) samples. In Section 4.1 of this paper, we compare our arm parameters with those of Yu & Ho (2020).

2.2. GZ-3D Masks

In the GZ-3D citizen science project (Masters et al. 2021), participants marked spiral arms and bars on the SDSS images of the GZ-3D galaxies. GZ-3D participants also marked the galaxy centers and foreground stars. For the spiral arm marking activity in GZ-3D, the targets were chosen from the subset of the MaNGA target galaxies previously classified in the earlier Galaxy Zoo 2 project to be spiral galaxies with ≤ 4 spiral arms. This selection criteria eliminates some of the most flocculent spiral galaxies as well as most ellipticals. This limits the sample of galaxies with available GZ-3D spiral arm masks to only 7418 out of the 29,831 galaxies in the full GZ-3D sample (Masters et al. 2021). Of these 7418 galaxies, 4449 meet our criteria of $z < 0.05$ and ellipticity ≤ 0.5 . This set of 4449 galaxies is called our low z GZ-3D spiral arm sample in the following.

Each galaxy in this list was viewed by at least 15 GZ-3D volunteers. Spiral arm masks were made for each galaxy based on the markings by the viewers. In the mask, each pixel in the image is set to an integer number between 0 to 15, where the count is equal to the number of volunteers that identified that pixel as belonging to a spiral arm. Similar masks were made for the volunteer markings of the bars. The GZ-3D masks have pixels $0''.099$ wide, and are 525×525 pixels ($52'' \times 52''$). This corresponds to a field of view of 11 kpc (54 kpc) on a side for the closest (most distant) galaxies.

2.3. Algorithm for Finding and Counting Arms

We use the GZ-3D masks to identify spiral arms in the galaxies. In our analysis, for a given pixel to count as being ‘on the arm’, we use a threshold of at least three counts, i.e., out of the 15 possible viewers, at least three participants (20%) selected that pixel as being on an arm. This threshold is recommended by Masters et al. (2021), who noted that this cutoff reveals continuous and distinct spiral patterns. We consider pixels in the ‘interarm’ as pixels which none of the participants labeled as being on the arm (i.e., count = 0). This is a conservative limit. The consequences of these criteria are discussed below.

We converted the pixel x,y coordinates into polar coordinates centered on the galaxy center, using the central position marked by the GZ-3D participants. When two or more galaxies are in the field of view and the nuclei were both marked by volunteers, we used the nucleus closest to the center of the image. We then stepped out in radius from that center in elliptical annuli, deprojecting the mask into the plane of the galaxy. We assume that the intrinsic shape of the disk in the plane of the galaxy is circular, and these elliptical annuli are projections from the plane of the sky to circles in the plane of the galaxy disk. For this deprojection, for the galaxies in the Yu & Ho (2020) sample, we used their determination of ellipticity and position angle rather than the NSA value as they are more accurate (Yu & Ho 2020). If the galaxy was not in Yu & Ho (2020), then we used the NSA elliptical Petrosian PA and ellipticity. For

each x,y position on the image, we calculated the azimuthal angle θ in the plane of the sky and the distance from the galaxy center in the plane of the galaxy.

We then stepped out in radius from the center in one pixel wide radial bins, searching for arms along each annulus. For each radial step we searched in azimuthal angle along the annulus, looking for pixels that exceed our nominal threshold level. After identifying an arm, we continue along the annulus, searching for a pixel that meets our interarm criteria. After finding interarm, we continue along the annulus searching for another pixel that exceeds the threshold for an arm, followed by an interarm pixel. Each independent ‘arm/interarm’ sequence along the annulus is defined as an independent arm at that radius. This means that each arm must have defined interarm pixels on either side of the arm in the annulus. If the entire annulus is above the interarm level of zero counts, then the arm count for that annulus is zero. Alternatively, if no pixels along the annulus exceeds the threshold, the arm count for that annulus is also zero. To identify an arm, there must be at least one pixel along the annulus at or above the threshold, and at least one pixel at the defined interarm level.

In stepping out in the galaxy, we started at a radius of 20 pixels ($1''.98$) from the center, and continued to a radius of 250 pixels ($24''.75$), stepping out 1 pixel at a time. In our final analysis, we only flag galaxies which have at least 10 radial steps with at least one arm by the above criteria. This means that galaxies with weak or no spiral arms, or very flocculent or ill-defined arms, are unflagged. Among the galaxies with ten radial steps with arms, we flagged a galaxy as a possible n-armed galaxy if at least four of the radial steps in a continuous sequence (i.e., at least $0''.396$ in radius) were found to have n arms by the above criteria, where $n = 1, 2, 3, 4$, and ≥ 4 . Note that the same galaxy can be flagged in more than one way if we find different arm counts in different 4-step sequences. An example would be a galaxy that is flagged as 2-armed for a given range of radius, and 3-armed for a different range of radius. Out of our initial sample of 4449 low z GZ-3D spiral arm galaxies, the number of galaxies flagged as 1-armed, 2-armed, 3-armed, 4-armed, and 5+arms, are 3965, 2806, 367, 23, and 3, respectively.

We flagged a subset of the ‘2-armed’ galaxies as ‘grand design’ spirals, if: a) only two arms were found in a continuous sequence of at least 50 radial steps ($4''.95$), and b) the galaxy was not flagged as 3-armed or 4-armed. Based on these criteria, we flagged a total of 402 galaxies as grand design.

In this section, we have outlined our attempt to use the superior pattern finding abilities of human observers to develop a consensus classification scheme. In the next section, we assess the reliability of our classifications.

2.4. *Visual Inspection of Images*

We used the ds9 software² to inspect by eye the SDSS g-band images of all of the galaxies flagged by our code as either grand design or as 3-armed. Since spiral arms show up more readily in blue images than red images, we used the g images for these inspections. Using ds9, we varied the greyscale display by hand for each galaxy, and inspected each galaxy carefully. We found that in some cases the GZ-3D spiral arm masks at a threshold = 3 do not trace arms as far out as can be seen by eye in the SDSS g image. Furthermore, sometimes multiple arms can be seen by eye in the galaxy, but not all of these arms are above the threshold=3 level in the GZ-3D mask. Also, in some cases a single GZ-3D volunteer marked a large portion of the disk as ‘arm’, causing arms in that region not to be found by our algorithm due to the lack of ‘interarm’ pixels in the mask.

However, from our inspection of the images we conclude that the arms that are found from the GZ-3D masks using our method with a threshold of 3 are generally reliable. The main shortcoming of our method is that sometimes additional fainter arms are missed, or the arms aren’t traced out as far on the image as can be seen by eye. That means that the arm counts from our software may be lower limits on the true arm counts for some galaxies. Inspection shows that most galaxies flagged as 3-armed by our code have at least three arms, and sometimes more arms. In other words, they comprise a robust sample of multi-armed galaxies.

We explored how our results would change if we set our definition of interarm to 1 count instead of zero. With this more relaxed definition, the code is able to recover more spiral arms, however, it sometimes gives false positives, i.e., it sometimes counts more arms than are visible by eye. Thus, for our final analysis we used the interarm = 0 criterion, which is more reliable although less complete.

The images were independently inspected by three of the co-authors. We divided them by eye into three groups: galaxies that ‘very likely’ belonged to the arm class the code selected, galaxies that ‘likely’ belonged to the class, and galaxies that may not belong to the class. The three sets of by-eye classifications were then merged into a single list.

² <https://sites.google.com/cfa.harvard.edu/saoimageds9>

If two or all three of the by-eye rankings of a particular galaxy agreed, then the galaxy was assigned to that group. If the three by-eye rankings were different, then the galaxy was placed in the middle ‘likely’ group. The individual by-eye rankings were reasonably consistent, with 92% of the galaxies having at least two of the three rankings the same. In comparing the properties of the multi-armed and grand design galaxies, we combine the ‘very likely’ and ‘likely’ galaxies together to make the final samples of galaxies. The final conclusions of this paper do not change if only the ‘very likely’ galaxies were included in the analysis.

Of the 367 galaxies flagged by the code as 3-armed, by eye we classified 202 (55%) as ‘very likely’ multi-armed and another 97 (26%) as ‘likely’ multi-armed. Together, this gives an overall estimated reliability of 81% for our automatic method of finding multi-armed galaxies, assuming that the consensus vote of our by-eye classifications is the correct classification. In other words, the code selects a sample of 3+ armed galaxies that is 85% ‘pure’ multi-armed galaxies. The remaining 15% are mostly galaxies that are dominated by 2-arms that are erroneously classified. These misclassifications include barred galaxies with two tightly-wrapped arms in a ring-like structure, where the code erroneously counted one arm twice, perhaps because the NSA ellipticity is somewhat inaccurate or the arm is distorted. After filtering out these incorrectly-classified galaxies by eye, our final set of visually-confirmed multi-armed galaxies contains 299 galaxies. We use these 299 galaxies in the following analysis.

Our sample of multi-armed galaxies includes galaxies with branching spiral arms, for example, galaxies with two dominant arms in the interior that bifurcate to produce four long arms in the outer disk. This morphology is common among galaxies classified as multi-armed (Buta et al. 2015). The Milky Way may have this structure (Minniti et al. 2021; Xu et al. 2023).

Because the GZ-3D masks sometimes miss spiral arms, the code sometimes under-counts the number of arms. This means that galaxies that are only flagged as ‘2-armed’ might in fact have three or more arms. Our strict definition of grand design galaxies, in which we require 50 radial steps in sequence with only 2 arms and exclude galaxies also flagged as 3-armed, improves the reliability of the classification, but it is not perfect. Of the 402 galaxies selected as grand design by our algorithm, 146 (36%) were seen by eye as ‘very likely’ grand design, and 99 (24%) were classified as ‘likely’ grand design, implying a 60% overall reliability. Some of these galaxies show short branching of the spiral arms in the outer disk, but overall they are dominated by two arms over the majority of the disk, thus we classify them as grand design for this study. The final set of 245 galaxies confirmed by eye to be likely/very likely grand design is used in the analysis below.

Although our method of finding multi-armed and grand design galaxies using the GZ-3D masks is reasonably reliable, the final samples are very incomplete. Out of the 4449 galaxies in the $z < 0.05$, ellipticity < 0.5 subset of the GZ-3D spiral arm sample, 3994 (90%) were initially flagged by our procedure. Of those 3994 galaxies, only a fraction (14%) ended up in either our final sample of 299 multi-armed galaxies or the final sample of 245 grand design galaxies. This incompleteness should be kept in mind in the following analysis.

In Appendix A of this paper, we provide some examples of galaxies identified as grand design and as multi-armed, show the GZ-3D masks for these galaxies, and illustrate our flagging procedure. In Appendix B, we investigate whether the limited field of view biases the final conclusions of this paper.

3. RESULTS

3.1. Arm Counts vs. Redshift and M^*

The MaNGA/GZ-3D selection criteria is illustrated in Figure 1, where we plot stellar mass (obtained from the NSA) vs. redshift. The galaxies in our final grand design sample are shown as blue open squares, and the multi-armed galaxies are marked by red filled triangles. The small black dots represent galaxies in the low z GZ-3D spiral arm sample that are not in our final GD or MA sample. Galaxies in the larger angular size ‘Primary’ MaNGA subset populate a broad band of galaxies extending from redshifts of about 0.02 at low masses to a redshift of 0.05 at high masses. The second band of galaxies at higher redshifts includes galaxies in the ‘Secondary’ sample, which have smaller angular sizes. The MaNGA ‘Color-Enhanced’ add-on sample of galaxies contributes to the scatter in the plot. Both grand design and multi-armed galaxies are seen in the full range of masses and redshifts of the sample.

In Figure 2, we provide histograms of the redshifts (left panel) and stellar masses (right panel) for our final sets of 245 grand design spirals and 299 multi-armed galaxies. The sample contains very few galaxies from $0.01 \leq z < 0.015$, followed by a broad peak from $z = 0.02 - 0.03$, a drop at around $z \sim 0.035$, followed by a flat plateau which ends abruptly at our redshift limit of 0.05. The drop-off at $z \sim 0.035$ is due to the gap between the primary and secondary samples as seen in Figure 1.

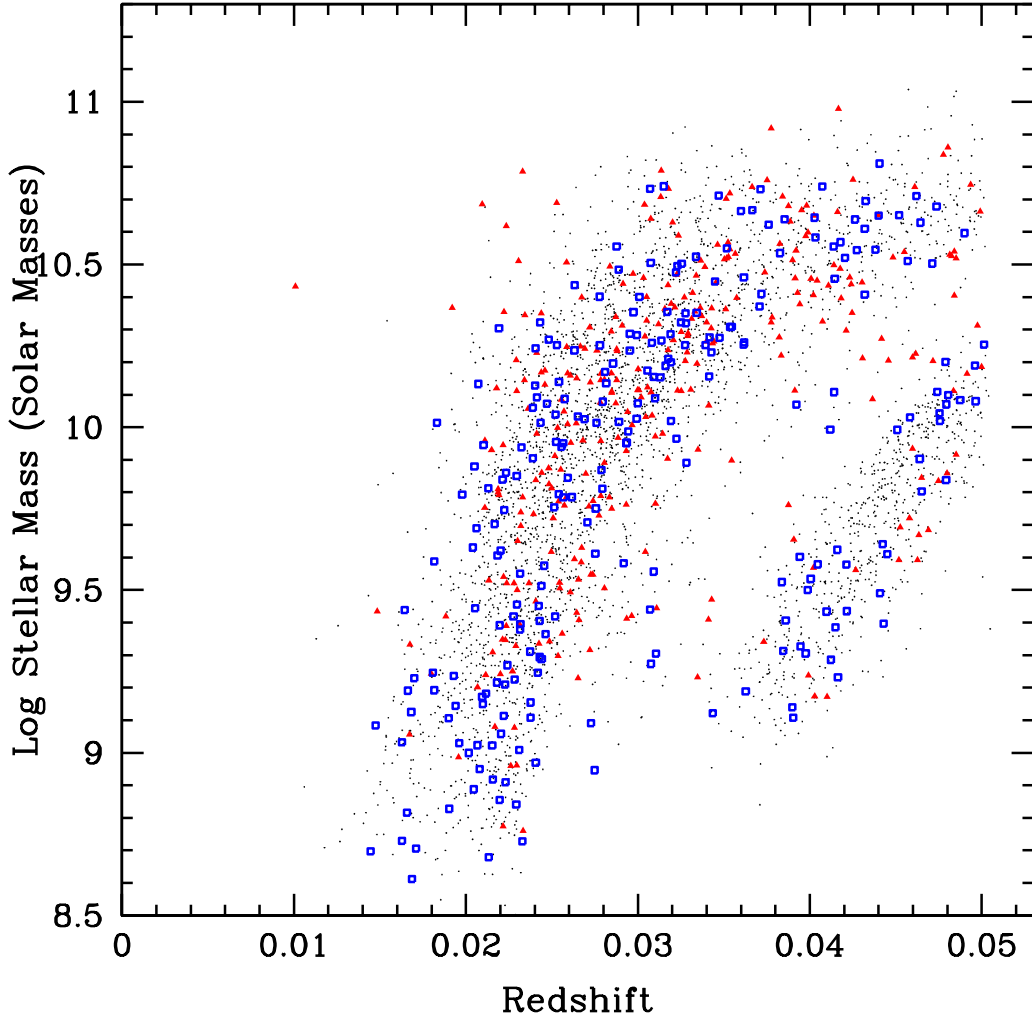


Figure 1. Stellar mass vs. redshift for our grand design (blue open squares) and multi-armed galaxies (red filled triangles). Other galaxies in our initial set of 4449 GZ-3D galaxies with $z < 0.05$, ellipticity ≤ 0.5 are marked by small black dots. The galaxies in the ‘Primary’ and ‘Secondary’ MaNGA subsets are separated into two ‘bands’ in this plot, with the larger angular size ‘Primary’ galaxies in the leftmost band.

In the following analysis, we use Kolmogorov-Smirnov (KS) and Anderson-Darling (AD) statistical tests to compare various properties of the multi-armed galaxies vs. the grand design galaxies. KS and AD tests give probabilities that

two samples came from the same parent sample, where a value greater than 0.05 means that there is no significant difference between the two samples. Our AD test implementation only provides a limit on the probability if it is above ≥ 0.25 or below 0.001. Both tests find a significant difference between the redshifts of the two samples (KS probability of 0.02; AD probability of 0.006). The grand design galaxies have a slightly broader distribution in z than the multi-armed galaxies, but a similar median z . When the sample is divided into subsets by M^* , a marginal difference remains in the $9 \leq \log(M^*/M_\odot) < 10$ bin (KS probability 0.055; AD probability 0.029), but no difference is seen for galaxies in the range $10 \leq \log(M^*/M_\odot) < 11$.

We see a clear difference in the stellar masses of our grand design vs. our multi-armed galaxies. The multi-armed galaxies have a mass distribution that is skewed to higher masses compared to the grand design galaxies (Figure 2, right), a result confirmed by KS and AD tests (KS probability of 0.00024, AD probability < 0.001).

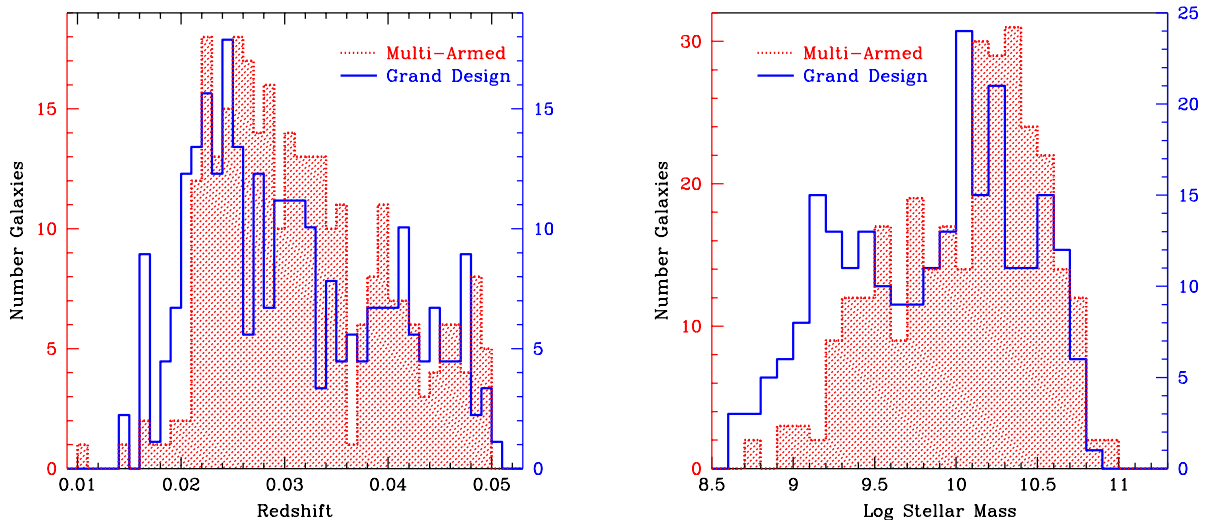


Figure 2. Histograms of redshifts (left panel) and stellar masses (right panel) for the final set of multi-armed galaxies (red hatched histogram) and grand design spirals (blue histogram). The left axis gives the number of galaxies for the multi-armed sample, while the right axis gives the number of grand design galaxies.

3.2. Arm Counts vs. Concentration

In this paper, we define concentration as the ratio of the radius containing 90% of the SDSS r band light (R_{90}) to the radius containing 50% of the light (R_{50}) (Strateva et al. 2001; Kauffmann et al. 2004), using the elliptical Petrosian radii from the NSA. In Figure 3 we show histograms of the concentrations for our sample of multi-armed galaxies vs. the grand design galaxies. KS/AD test results for various stellar mass ranges are given in Table 1. Galaxies identified as multi-armed have significantly lower concentrations on average than the grand design galaxies. This difference holds even when the galaxy is divided into subsets by mass, except for the lowest mass bin ($9.1 \leq \log(M^*/M_\odot) < 9.4$).

Concentration is a function of stellar mass for spiral galaxies, in that galaxies with higher masses tend to have larger concentrations. This trend is shown in Figure 4, where we plot concentration vs. stellar mass for both the multi-armed and grand design galaxies. A reasonably strong correlation is seen between mass and concentration for the grand design galaxies, while the correlation is weaker for the multi-armed galaxies. Figure 4 shows a deficiency of high mass, low concentration galaxies in the grand design sample, compared to the multi-armed sample.

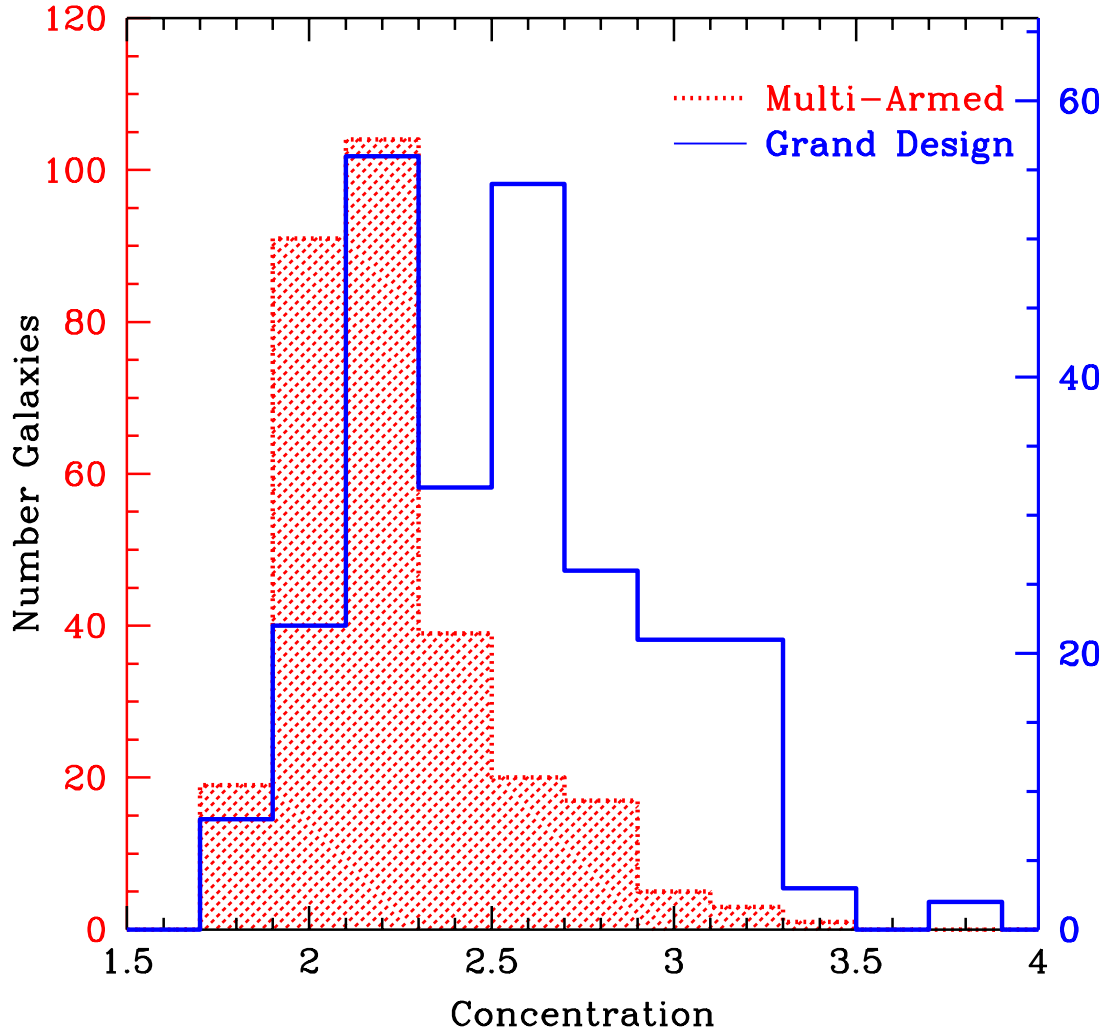


Figure 3. Histograms of the concentrations for our multi-armed (red hatched) vs. grand design galaxies (blue). Concentration is defined as the ratio of R_{90}/R_{50} , where R_{90} and R_{50} are the radii containing 90% and 50% of the SDSS r band light, respectively, using elliptical Petrosian radii from the NSA. The left axis gives the number of galaxies for the multi-armed sample, while the right axis gives the number of grand design galaxies.

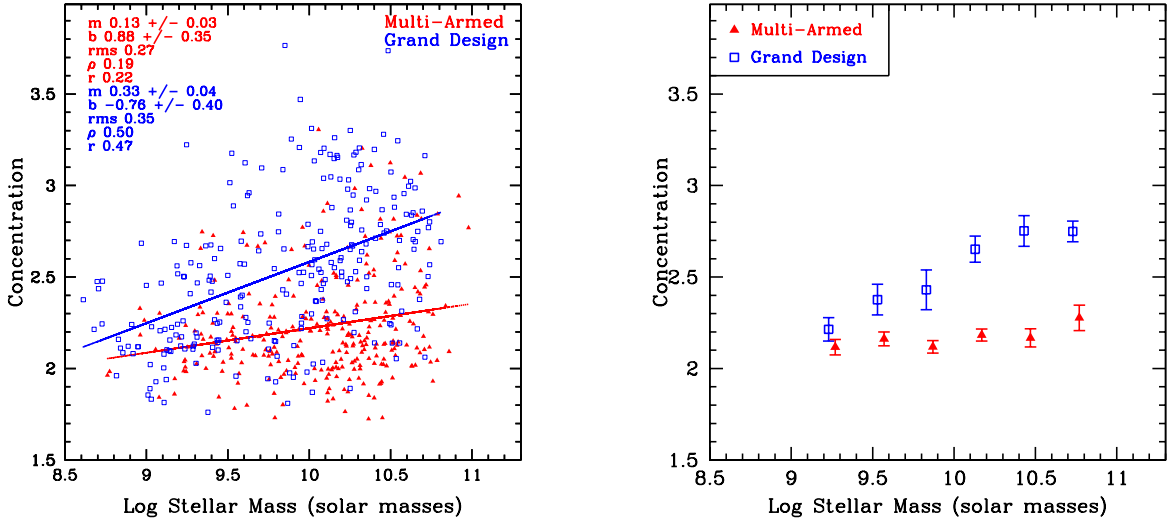


Figure 4. Left: Plot of concentration vs. stellar mass for galaxies in our multi-armed galaxy sample (red filled triangles) and galaxies classified as grand design (blue open squares). Concentration is defined as the ratio of R_{90}/R_{50} , where R_{90} and R_{50} are the radii containing 90% and 50% of the SDSS r band light, respectively, using elliptical Petrosian radii from the NSA. The red line is the best-fit for the multi-armed galaxies, while the blue line is the best-fit for the grand design galaxies. The best-fit slope (m), y-intercept (b), and rms for the two sets of galaxies are displayed in the corresponding color, along with the Spearman (ρ) and Pearson (r) correlation coefficient. Right: plot of median concentration for the grand design galaxies (open blue squares) and the multi-armed galaxies (red filled triangles) in bins in $\log M^*$. The error bars give the error in the median $\sim \text{IQR}/\sqrt{N}$, where IQR is the inter-quartile range and N is the number of datapoints in that set. The red and blue datapoints are slightly offset from the center of the mass bin to make the data easier to see. Results of KS/AD tests comparing the grand design and the multi-armed galaxies in each mass bin are given in Table 1.

In the right panel of Figure 4, we plot the median concentrations from Table 1 for grand design galaxies (blue open squares) and multi-armed galaxies (filled red triangles) within 0.3 dex bins in M^* . Significant differences are present in all mass bins except possibly the lowest mass bin.

3.3. Arm Counts vs. Physical Size

In Figure 5, we plot two different estimates of galaxy size vs. stellar mass, for our two classes of spiral galaxies. The left panel shows the log of the SDSS r band R_{50} radius (half light radius) from the NSA vs. $\log M^*$, while the right panel displays $\log R_{90}$ vs. $\log M^*$. For R_{50} , the slope of the best-fit line is significantly steeper for the multi-armed galaxies compared to that for the grand design galaxies (left panel, Figure 5). Above $\log(M^*/M_{\odot}) > 10$, there is a clear offset between the two classes of spiral galaxies, with multi-armed galaxies having larger R_{50} for a given stellar mass. The correlation between $\log R_{50}$ and $\log M^*$ is stronger for the multi-armed galaxies. For R_{90} , the difference between grand design and multi-armed galaxies is smaller; the slope of the best-fit line for multi-armed galaxies is only marginally larger than that of grand design galaxies. In Figure 5, there is a hint of a bend in the relation near $\log(M^*/M_{\odot}) = 10$, with a steeper slope at higher masses.

These plots show that the total extent of stellar disks in the two classes of spirals are similar for a given stellar mass; the differences in concentration (R_{90}/R_{50}) between the two classes of galaxies are associated with grand design galaxies having smaller R_{50} values for a given R_{90} size than multi-armed galaxies, meaning they have proportionally more light in the center.

Table 1. Kolmogorov-Smirnov/Anderson-Darling Tests: Comparing Concentration for Multi-Armed vs. Grand Design Galaxies

| Log M* Range (M _⊙) | Number Multi- Armed Galaxies | Number Grand Design Galaxies | KS/AD Prob | Multi-Armed | | | Grand Design | | |
|---|---------------------------------------|---------------------------------------|----------------------------------|-------------|----------------------|----------------------|--------------|----------------------|----------------------|
| | | | | Median C | 1st Quartile C | 3rd Quartile C | Median C | 1st Quartile C | 3rd Quartile C |
| 10 to 11 | 180 | 116 | $8 \times 10^{-22} / \leq 0.001$ | 2.19 | 2.04 | 2.42 | 2.69 | 2.49 | 2.98 |
| 10 to 10.5 | 128 | 82 | $9 \times 10^{-20} / \leq 0.001$ | 2.18 | 2.02 | 2.35 | 2.68 | 2.5 | 3.04 |
| 10.5 to 11 | 52 | 34 | $0.0001 / \leq 0.001$ | 2.28 | 2.11 | 2.59 | 2.7 | 2.46 | 2.91 |
| 9.1 to 9.4 | 23 | 39 | 0.075/0.034 | 2.12 | 2.02 | 2.22 | 2.21 | 2.11 | 2.5 |
| 9.4 to 9.7 | 38 | 32 | $0.01 / \leq 0.001$ | 2.16 | 2.07 | 2.3 | 2.38 | 2.18 | 2.66 |
| 9.7 to 10.0 | 50 | 33 | $0.00093 / \leq 0.001$ | 2.12 | 2.04 | 2.28 | 2.43 | 2.13 | 2.75 |
| 10 to 10.3 | 73 | 60 | $6 \times 10^{-14} / \leq 0.001$ | 2.18 | 2 | 2.28 | 2.65 | 2.48 | 3.03 |
| 10.3 to 10.6 | 77 | 37 | $2 \times 10^{-7} / \leq 0.001$ | 2.17 | 2.07 | 2.51 | 2.75 | 2.46 | 2.97 |
| 10.6 to 10.9 | 28 | 19 | $0.00012 / \leq 0.001$ | 2.28 | 2.09 | 2.46 | 2.75 | 2.61 | 2.86 |

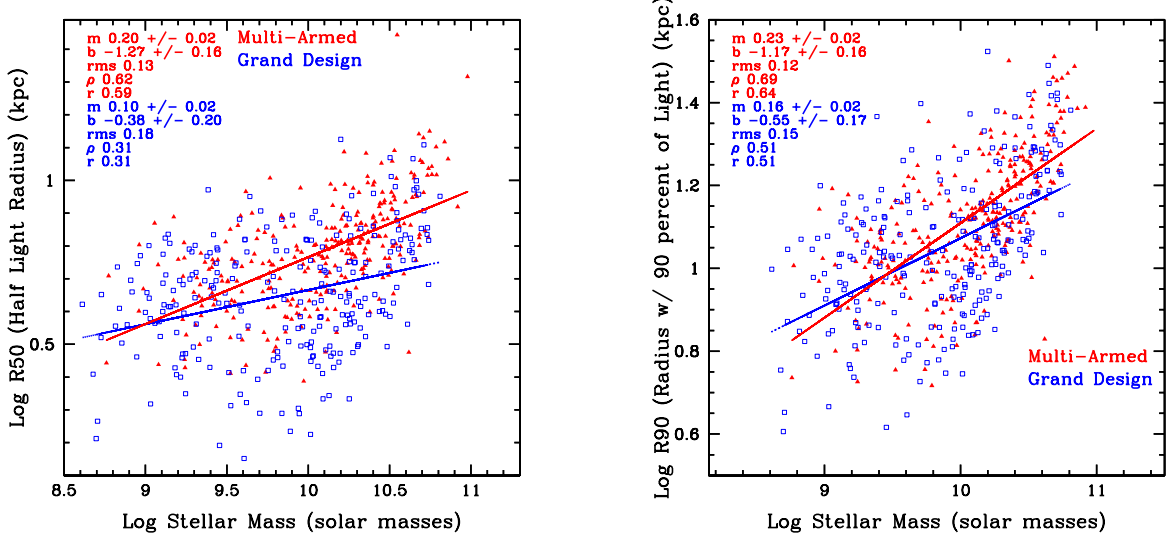


Figure 5. Left: Plot of the log of the SDSS r band R50 radius (half light radius) from the NSA vs. the log of the stellar mass, for our multi-armed (red filled triangles) and grand design galaxies (blue open squares). Right: Plot of R90, the radius containing 90% of the SDSS r band light, vs. the stellar mass for our sample of multi-armed galaxies (red filled triangles) and the grand design galaxies (blue filled squares). The red lines are the best-fit linear relations for the multi-armed galaxies, while the blue lines are the best-fit lines for the grand design galaxies. The parameters of the best-fit lines and the Spearman (ρ) and Pearson (r) correlation coefficients are overlaid in the corresponding color.

3.4. Arm Count vs. Hubble Type

For many galaxies in the NSA, Domínguez Sánchez et al. (2018) used machine learning with Convolutional Neural Networks to estimate their TType, where TTypes are Hubble types coded into numerical values. Their code was trained using the Nair & Abraham (2010) by-eye classifications of Hubble Types as well as GZ2 classifications from Willett et al. (2013). In the left panel of Figure 6, we provide histograms of the Domínguez Sánchez et al. (2018) TTypes for our final samples of multi-armed and grand design galaxies. The distribution of TTypes for the grand design galaxies is skewed toward earlier-type galaxies compared to the multi-armed galaxies. KS and AD tests for the full mass range confirm that there is a significant difference in TTypes between the two samples (KS probability 0.0047, AD probability 0.002).

Like concentration, TType also depends upon mass. In the right panel of Figure 6, we plot TType vs. stellar mass for our multi-armed and grand design galaxies. For both arm classes, there is a strong correlation, in that lower mass galaxies have later TTypes. For a given stellar mass, the grand design galaxies tend to have earlier types, however, the slopes of the best-fit relations are consistent within the uncertainties. When the sample is sub-divided by stellar mass into 1 dex bins, a difference in TType is seen in the $10 \leq \log (M^*/M_\odot) < 11$ bin (KS probability 0.0023, AD probability ≤ 0.001) but not in $9 \leq \log (M^*/M_\odot) < 10$. Sub-dividing further into 0.3 dex bins, only the $10 \leq \log (M^*/M_\odot) < 10.3$ bin shows a significance difference (KS probability 0.0023, AD probability ≤ 0.001), with the median TType for grand design galaxies being less than for multi-armed galaxies.

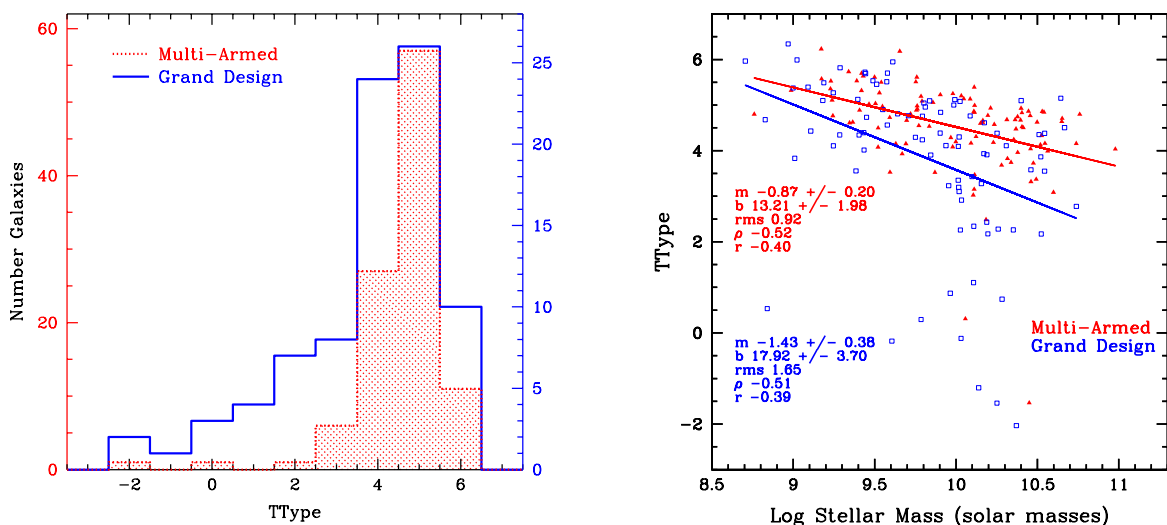


Figure 6. Histograms of the Domínguez Sánchez et al. (2018) Hubble Type (TType) for our multi-armed (red hatched) and grand design galaxies (blue). The left axis gives the number of galaxies for the multi-armed sample, while the right axis gives the number of grand design galaxies. Right: Plot of the Domínguez Sánchez et al. (2018) Hubble Type (TType) vs. log stellar mass for our multi-armed galaxies (red filled triangles) and grand design galaxies (blue open squares). The best-fit line for the multi-armed galaxies is plotted in red, while the best-fit line for the grand design galaxies is given in blue. The parameters of the best-fit line are given in the corresponding color.

3.5. Arm Counts vs. Central Surface Mass Density

Measurements of the surface mass density within the central 1 kpc radius (Σ_1) are available from Luo et al. (2020) for 209 of our multi-armed galaxies and 135 of our grand design galaxies. In the left panel of Figure 7, we plot $\log \Sigma_1$ against $\log M^*$ for both classes of spirals. In both cases, Σ_1 is correlated with M^* . However, grand design galaxies

show a steeper slope for the best-fit line, and an offset is seen between the two arm classes at high masses; for a given M^* , grand design galaxies have higher Σ_1 on average.

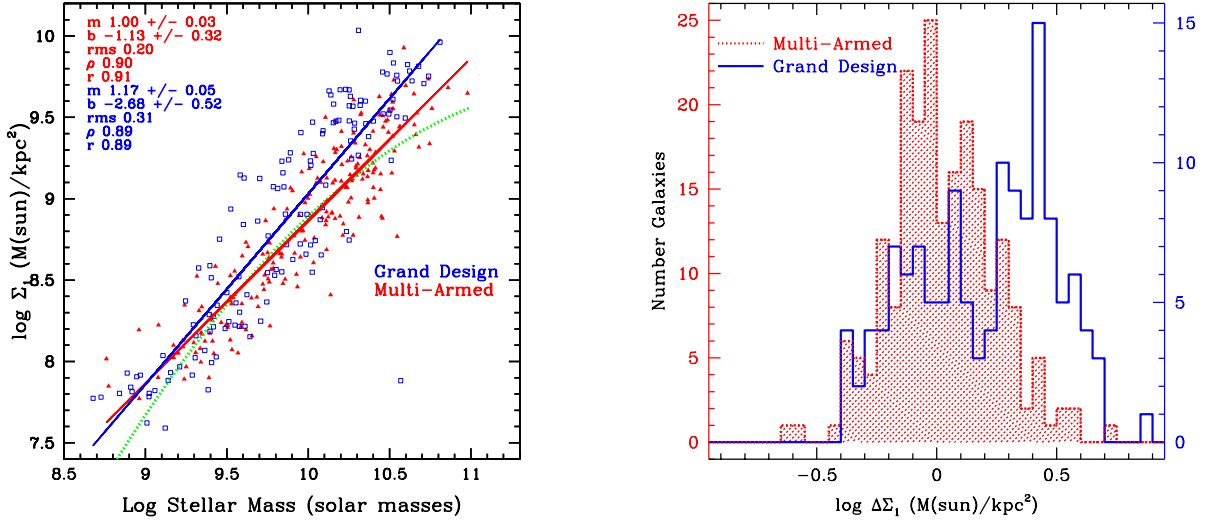


Figure 7. left: Plot of $\log \Sigma_1$ vs. $\log M^*$ for the multi-armed (red filled triangles) and grand design (blue open squares) galaxies. The red line is the best-fit line for the multi-armed galaxies; the blue line is the best-fit line for the grand design galaxies. The parameters of the fits are given in the corresponding colors. The green dotted curve is the Luu et al. (2020) dividing line between galaxies with classical bulges (above the curve) and pseudo-bulges (below). Right: $\log \Delta \Sigma_1$ for multi-armed (red hatched) and grand design (blue) galaxies, where $\log \Delta \Sigma_1$ is defined by Luu et al. (2020) as the offset from the green curve in the left panel. Galaxies that lie to the right of zero in these histograms lie above the green curve in the plot on the left. The left axis gives the number of galaxies for the multi-armed sample, while the right axis gives the number of grand design galaxies.

Luu et al. (2020) concluded that Σ_1 is related to bulge type; galaxies with bulges classified as pseudo-bulges have lower Σ_1 for a given M^* than galaxies with classical bulges. A pseudo-bulge is a disk-like structure in the center of a spiral galaxy that masquerades as a bulge and was produced by secular processes, while a classical bulge resembles an elliptical embedded within a disk galaxy (Kormendy & Kennicutt 2004). In the left panel of Figure 7, we overlay the dividing curve between the two classes of bulges as determined by Luu et al. (2020). Proportionally more grand design galaxies lie above the Luu et al. (2020) curve, relative to the multi-armed galaxies.

In the right panel of Figure 7, we provide histograms of $\log \Delta \Sigma_1$, where $\log \Delta \Sigma_1$ is defined by Luu et al. (2020) as the offset in $\log \Sigma_1$ from the green line in the left panel of Figure 7. With this definition, according to Luu et al. (2020) $\log \Delta \Sigma_1$ is positive for galaxies with classical bulges, and negative for galaxies with pseudo-bulges. Figure 7 shows that a larger fraction of grand design galaxies have $\log \Delta \Sigma_1 > 0$ compared to multi-armed galaxies. A KS test gives a probability of only 3×10^{-10} that the two distributions of $\Delta \Sigma_1$ come from the same parent population. Using a cutoff of $\log \Delta \Sigma_1 = 0$ as the dividing line between the two bulge types, 70% of the grand design galaxies host classical bulges, but only 50% of the multi-armed galaxies. This result is discussed further in Sections 5.1.4 and 5.2.

3.6. Arm Count vs. Specific Star Formation Rate

In Figure 8, we compare the sSFRs for our multi-armed and grand design galaxies. For this analysis, we use sSFRs from the GALEX-Sloan-Wise Legacy Catalog version 2 (GSWLC-2) (Salim et al. 2016, 2018). Over the whole sample we see no significant difference in sSFR for the two classes (KS/AD probabilities 0.21/0.057). However, the sSFR of spirals is a function of stellar mass and concentration (Smith et al. 2022a). To determine how sSFR depends upon

the number of arms, it is important to separate out the effect of M^* and C . In the left panels of Figure 8, we plot \log sSFR vs. $\log M^*$ for the two classes of galaxies (top panel: grand design; bottom panel: multi-armed). Galaxies with lower stellar masses tend to have higher sSFRs. In the left panels of Figure 8, the galaxies are further divided into two sets based on concentration. The best-fit linear relations for these subsets are shown. For the grand design galaxies, galaxies with larger concentrations have lower sSFRs on average than galaxies with smaller concentrations. For multi-armed galaxies, the best-fit \log sSFR vs. $\log M^*$ relation for high C and low C galaxies are reasonably consistent.

In the right panel of Figure 8, we plot the median sSFR of grand design and multi-armed galaxies in 0.5 dex wide bins in M^* , after dividing into two bins in concentration. We ran KS and AD tests on these subsets. The only bin for which a marginally significant difference is seen is the $9.5 \leq \log(M^*/M_\odot) < 10$, $1.55 \leq C < 2.65$ bin, with the multi-armed galaxies having a higher median sSFR. When we account for differences in concentration between grand design and multi-armed galaxies, we cannot rule out that sSFR is independent of the number of arms in a galaxy.

We repeated this analysis using $\log \Delta\Sigma_1$ rather than concentration. We divided the galaxies into five bins in M^* and two bins in $\log \Delta\Sigma_1$, and compared the sSFRs of the multi-armed and grand design galaxies in those bins. Only in the $9.0 \leq \log(M^*/M_\odot) < 9.5$, $\log \Delta\Sigma_1 < 0$ bin did we find that the multi-armed galaxies have significantly higher sSFRs than the grand designs (KS probability = 0.006). However, there are very few galaxies in that bin (14 of each kind), so this result is uncertain. With the current data, we cannot rule out that sSFR is independent of the number of arms, except indirectly via the correlation of sSFR with concentration, $\log \Delta\Sigma_1$, and mass.

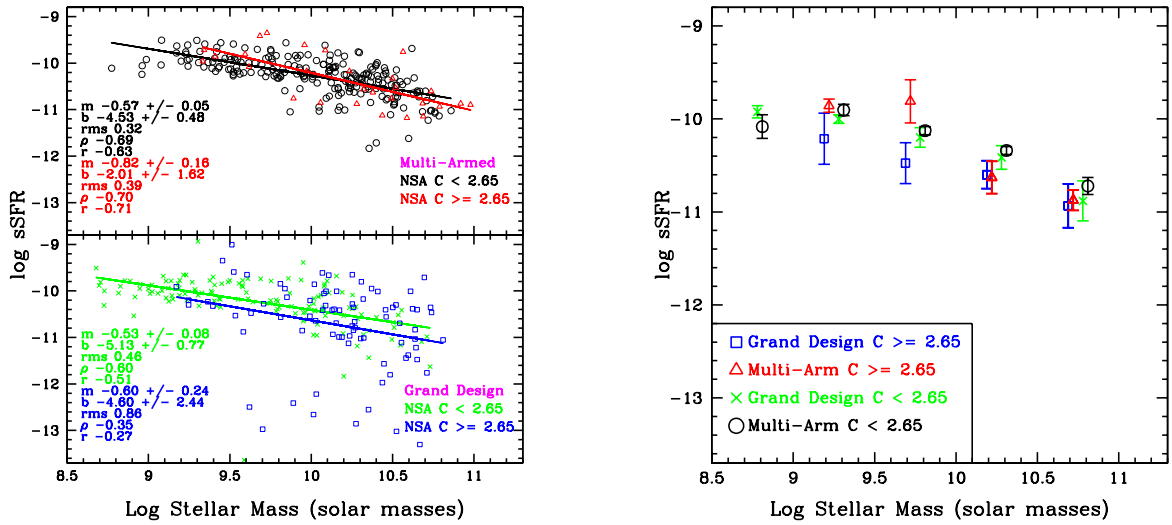


Figure 8. Plots of the \log of the sSFR vs. $\log M^*$. The left panels show the positions of individual galaxies, with grand design galaxies in the top panel and multi-armed galaxies in the bottom panel. In the panels on the left, the best-fit line for each subset and its parameters are shown in the corresponding color. The right panel gives the median sSFR for each subset as a function of $\log M^*$, within 0.3 dex bins in $\log M^*$. The sample is split into four subsets: blue open squares: grand design, NSA $C \geq 2.65$; green crosses: grand design, NSA $C < 2.65$; red open triangles: 3-armed, NSA $C \geq 2.65$; black open circles: 3-armed, NSA $C < 2.65$. In the right panel, the four subsets for a given $\log M^*$ are slightly shifted along the x-axis for ease in viewing. The error bars in the right panel give the error in the median $\sim IQR/\sqrt{N}$, where IQR is the inter-quartile range and N is the number of datapoints in that set. Only for the low C $9.5 \leq \log(M^*/M_\odot) < 10$ bin is there a marginally significant difference between the grand design and multi-armed galaxies, and only for the KS test.

4. COMPARISONS WITH PUBLISHED ARM COUNTS

4.1. Comparison with Yu & Ho (2020) Data

In this section, we compare our arm classes with arm parameters from the Yu & Ho (2020) survey, for galaxies in common between the two samples. Of the 1002 galaxies that are in both the GZ-3D and the Yu & Ho (2020) samples, 56 are in our final sample of multi-armed galaxies and 16 are in our final sample of grand design galaxies. In the left panel of Figure 9, we compare histograms of f_3 for galaxies in our multi-armed sample vs. galaxies in the grand design sample. Multi-armed galaxies have significantly larger f_3 values than grand design galaxies (KS probability 4×10^{-5}). The smaller f_3 values for the grand design galaxies are consistent with expectations, since grand design galaxies are expected to be dominated by the $m=2$ Fourier component, and thus have low f_3 values. This agreement supports the idea that our method of separating grand design and multi-armed galaxies is reliable.

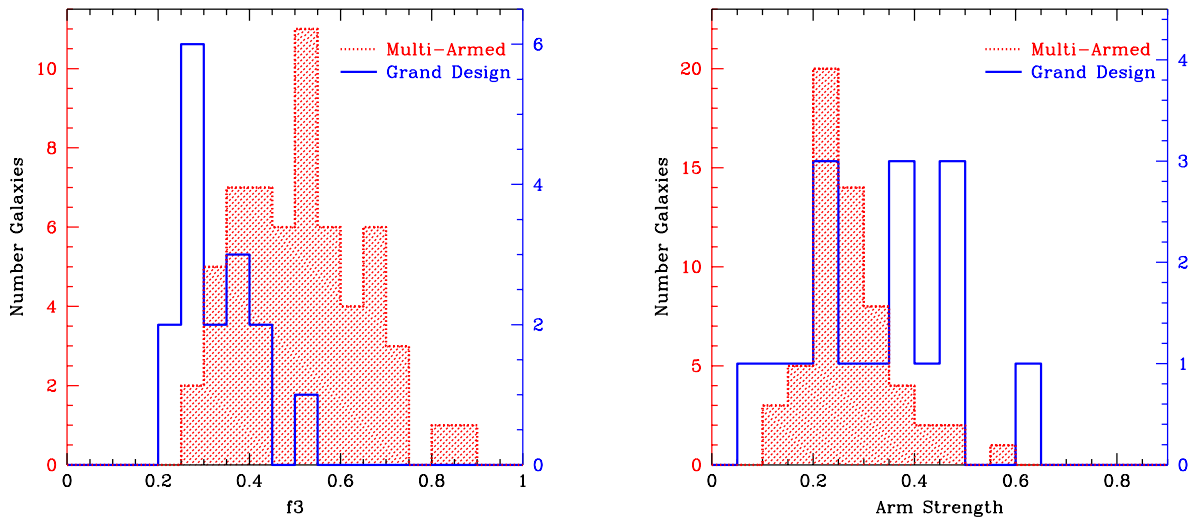


Figure 9. Left panel: Histograms of the Yu & Ho (2020) f_3 parameter for our multi-armed galaxies (red hatched) and grand design galaxies (blue). Right panel: Histograms of the Yu & Ho (2020) arm strengths for our multi-armed (red) and grand design (blue) galaxies.

In the right panel of Figure 9, we provide histograms of the Yu & Ho (2020) arm strengths for the multi-armed vs. grand design galaxies. The KS probability is 0.074, thus we cannot rule out that the two distributions come from the same parent sample. Histograms of the Yu & Ho (2020) pitch angles for our multi-armed vs. grand design galaxies are given in the left panel of Figure 10. While the range of pitch angle is large for each class, the median pitch angle is lower for the grand design galaxies. This implies that they tend to be more tightly wound than the multi-arm galaxies. This trend may be a consequence of the relation between concentration and number of arms (Figure 3), and an underlying correlation between pitch angle and concentration (Yu & Ho 2020). At any rate, the difference is marginally significant (KS probability 0.035).

4.2. Comparison with Galaxy Zoo 2 Arm Count Vote Fractions

We also compared our arm counts with the results of the Galaxy Zoo 2 (GZ2) citizen scientist project (Willett et al. 2013). Galaxy Zoo 2 asked participants a series of questions about each galaxy. First, participants were asked whether the galaxy is ‘smooth’, has ‘features/disk’, or has an ‘artifact’. If ‘features/disk’ was chosen, then they were asked if it is an edge-on disk. If ‘not edge-on’ was selected, then participants were asked whether the galaxy has spiral arms. If

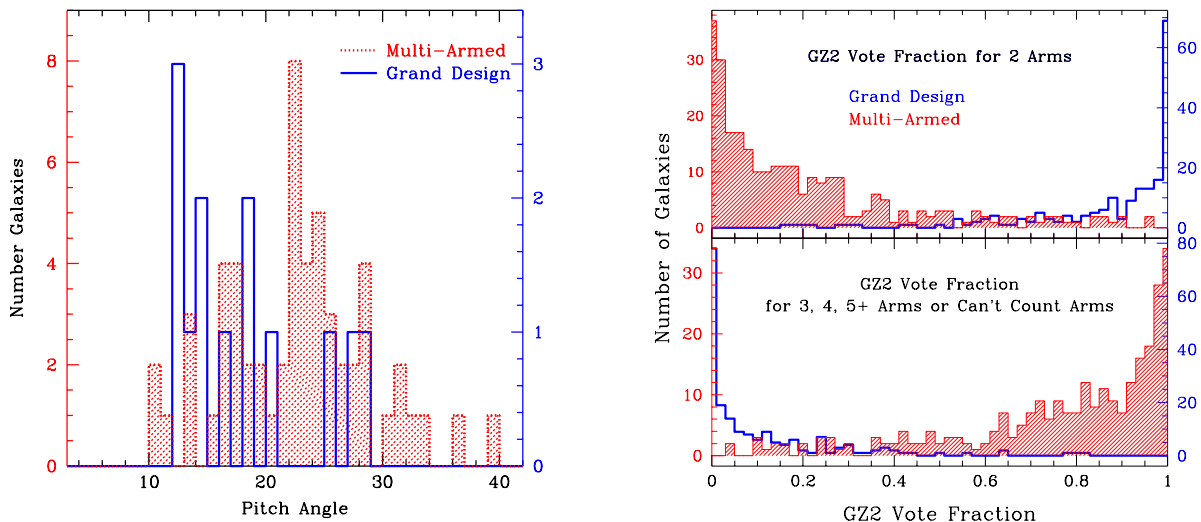


Figure 10. Left: Histograms of the Yu & Ho (2020) pitch angle for galaxies in our multi-armed galaxies (red hatched) and our grand design galaxies (blue). Right: Histograms of the GZ2 vote fraction for 2 arms (top panel) and for either 3 arms, 4 arms, 5+ arms, or ‘can’t count arms’ (bottom panel) for galaxies in our grand design sample (blue) and our multi-armed sample (red hatched). Only ‘secure spirals’ according to the definition of Willett et al. (2013) which have at least 20 classifications in GZ2 are included in the histograms on the right.

the participant said spiral arms were present, they were then asked how many spiral arms are present, with the choices being 1, 2, 3, 4, or 5+, or ‘can’t count arms’.

Hart et al. (2016) define a ‘secure spiral’ as a galaxy for which $p_{\text{feature}} \times p_{\text{not edge-on}} \times p_{\text{spiral}} > 0.5$, where p_{feature} is the fraction of votes in GZ2 for features/disk, $p_{\text{not edge-on}}$ is the fraction of votes for not being edge-on, and p_{spiral} the fraction of votes for having spiral arms. Of our set of 299 multi-armed and 245 grand design galaxies, 272 and 194, respectively, meet this condition and have at least 20 classifications votes in GZ2.

In the top right panel of Figure 10, for our multi-armed and grand design galaxies that meet these criteria, we display histograms of the fraction of the GZ2 volunteers who selected ‘2 arms’ in GZ2, while the bottom right panel shows the fraction who selected either ‘3 arms’, ‘4 arms’, ‘5+ arms’, or ‘can’t count arms’. This comparison shows that the vast majority of GZ2 viewers agreed that the grand design galaxies have two arms, while the majority of the GZ2 voters selected either 3 arms, 4 arms, 5+ arms, or ‘can’t count arms’ for our multi-armed galaxies. This shows good consistency between our method of counting spiral arms and the GZ2 statistics.

5. DISCUSSION

5.1. Comparison with Earlier Studies

We developed an algorithm for using GZ-3D masks to count the number of spiral arms as a function of radius within galaxies, and created a catalog of 299 multi-arm galaxies and 245 grand design galaxies. For galaxies that overlap with other studies, our classifications are in reasonable agreement with previous classifications. We compared the concentrations, stellar masses, Hubble types, central surface mass densities, and sSFRs of our two classes of spirals, and reached a number of conclusions. In this section, we compare our main conclusions to those of past studies.

In this study, we focus on grand design vs. multi-arm galaxies, and do not specifically target flocculent galaxies or treat them as a separate class. Our initial target list, the GZ-3D sample, explicitly excludes galaxies identified by GZ2 viewers as having more than four arms, thus our initial selection criteria was biased against flocculent galaxies.

Furthermore, our requirement that the GZ-3D masks have continuous radial sequences with the same number of arms also biases the search against fragmented arms. Some galaxies traditionally classified as flocculent may have ended up in our final multi-armed sample, although based on our by-eye inspection of the images the percentage of true flocculent galaxies in our multi-armed sample is relatively small. In our visual inspections of the images, we noted that many galaxies in both the grand design and the multi-armed sample appear clumpy in the SDSS g images, probably because of prominent knots of star formation along the spiral arms. It is possible that some of the galaxies we classified as multi-armed might be judged to be flocculent by other researchers, since the distinction between multi-armed and flocculent morphology is somewhat subjective. This point should be kept in mind in the following discussion, where we compare our results with the results of earlier studies in which arm classes were determined by eye.

5.1.1. Arm Counts vs. Concentration and Hubble Type

We see clear differences in the concentrations of the grand design and the multi-armed galaxies in our sample. For a given stellar mass, grand design galaxies tend to have larger concentrations compared to multi-armed galaxies. This difference in C becomes particularly pronounced at stellar masses greater than $10^{10} M_{\odot}$. Compared to multi-armed galaxies, there is a deficiency of high mass, low concentration grand design galaxies in our sample. For both the multi-armed and the grand design galaxies, we see a trend towards earlier Hubble types for larger stellar masses.

Our conclusion that grand design galaxies have larger concentrations and earlier Hubble types than multi-armed galaxies agrees with most earlier studies on the topic (Elmegreen & Elmegreen 1982; Bittner et al. 2017; Yu & Ho 2020) but not all (Ann & Lee 2013). In the original formulation of the arm class system as presented by Elmegreen & Elmegreen (1982), spiral galaxies were divided into 12 classes based on arm morphology. Classes 1 – 4 are varieties of flocculent galaxies, while classes 10 – 12 are classical 2-armed grand design galaxies. Galaxies in classes 5 – 9 include systems similar to those we label multi-armed galaxies in this study. For their sample of 305 spiral galaxies, Elmegreen & Elmegreen (1982) plot Hubble type vs. their 12 arm classes in their Figure 1. The flocculent galaxies in classes 1 – 4 tend to be very late types, while class 12, the most common of the grand design galaxies, tend to have earlier types. Arm classes 5 and 9, the most common types in their class 5 – 9 range, have Hubble types between those of the flocculent galaxies and the grand design galaxies. This is consistent with our results on the Hubble types of grand design vs. multi-armed galaxies. Many of our multi-armed galaxies have morphologies consistent with the Elmegreen & Elmegreen (1982) arm class 9 definition (‘multiple long arms in the outer parts, two symmetric and continuous arms in the inner parts’) or arm class 5 definition (‘two symmetric short arms in the inner regions; irregular arms in the outer regions’).

For a sample of 1064 nearby spiral galaxies classified by eye, Bittner et al. (2017) found statistically-significant differences in the TTypes of their grand design, multi-armed, and flocculent galaxies. Their grand design galaxies have the lowest TTypes, followed by multi-armed galaxies, with flocculent galaxies having the highest TTypes. Excluding their flocculent galaxies, our results are consistent with theirs.

Ann & Lee (2013) visually classified a set of 1725 SDSS spiral galaxies with $z < 0.02$ into grand design, flocculent, and multi-armed galaxies. In contrast to our results and the results of Buta et al. (2015), their grand design galaxies have similar or slightly smaller concentrations than their multi-armed galaxies. Ann & Lee (2013) also found that the distribution of Hubble types for their multi-armed galaxies tended to be peaked at earlier types than the distribution for grand design galaxies, also inconsistent with our results. This difference may be due to different ranges in M^* . Their SDSS sample is limited to angular sizes greater than $10''$, and otherwise is complete to about an absolute magnitude in r of $M_r = -16.1$. To convert this absolute magnitude into an approximate stellar mass, we derived a best-fit linear relation between $\log M^*$ and M_r for all field galaxies in the NSA of $\log (M^*/M_{\odot}) = -0.49 M_r + 0.03$. We defined field galaxies as galaxies that are not within 10 Mpc of the center of any Lim et al. (2017) group or cluster with a halo mass greater than $10^{12.5} M_{\odot}$ and more than four members. From this relation, we estimate that the Ann & Lee (2013) absolute magnitude limit corresponds to about $\log (M^*/M_{\odot}) = 7.9$. Their sample thus extends to lower stellar masses than our sample. Since both TType and concentration depend upon stellar mass (Figures 4 and 6), their sample may be skewed to later types and smaller concentrations than our sample. At the low mass end, there is less difference in C between multi-armed and grand design galaxies (Figure 4). The inclusion of very low mass galaxies in the Ann & Lee (2013) sample may explain why they found different concentration and TType distributions relative to our sample.

Our results on concentration agree with those of Yu & Ho (2020), who found a weak anti-correlation between the normalized $m=3$ Fourier amplitude f_3 and concentration. This implies that galaxies with larger bulges are more likely to have two symmetric arms.

5.1.2. Arm Counts vs. Stellar Mass

A second major conclusion of our paper is that grand design galaxies tend to have smaller stellar masses than multi-armed galaxies. This result agrees with earlier GZ2 studies. Using GZ2 arm counts for galaxies with $9 \leq \log (M^*/M_\odot) < 11$, Porter-Temple et al. (2022) found that multi-armed galaxies with 3, 4, or more arms tend to have higher stellar masses than 2-armed galaxies. In an earlier GZ2 study focused on high mass galaxies ($\log (M^*/M_\odot) \geq 10.6$), Hart et al. (2016) found that the fraction of spirals that are multi-armed increased with M^* relative to 2-armed galaxies. We find a peak in the ratio of the number of multi-armed galaxies to the number of grand design galaxies at $\log (M^*/M_\odot) = 10.3 - 10.6$ (see Appendix B), although the ratio drops off at higher M^* .

Our result on stellar masses differs from that of Bittner et al. (2017), however. For their sample of 1064 galaxies classified by eye into the three basic arm classes, Bittner et al. (2017) found no significant difference between the stellar masses of their multi-armed and grand design galaxies. The difference may be sample selection. Their sample is a subset of a volume-limited, magnitude-limited, and angular-size-limited sample (distance < 40 Mpc, B magnitude < 15.5 , $D_{25} > 1'$). Most of their galaxies lie between $9 \leq \log (M^*/M_\odot) < 10$, with only a relatively small fraction above $\log (M^*/M_\odot) = 10$. Our galaxies are more distant, with larger masses on average.

5.1.3. Size vs. Stellar Mass Relations

Our grand design galaxies have a flatter $\log R50$ vs. $\log M^*$ relation than the multi-armed galaxies. At higher masses, the grand design galaxies have smaller R50 for a given M^* than multi-armed galaxies. In Figure 11, we compare our datapoints and our best-fit relations to those of earlier r-band studies. For a sample of 8399 galaxies in the GAMA survey with $0.01 < z < 0.1$, Lange et al. (2015) fit $\log R50$ vs. $\log M^*$ for ellipticals and non-ellipticals. The slope of their best-fit relation for the non-ellipticals (0.20 ± 0.02) is the same as ours for the multi-armed galaxies, however, their line is offset to lower radii. Their elliptical galaxies show a steeper slope, but for $\log (M^*/M_\odot) < 11$ the ellipticals have significantly smaller effective radii than non-ellipticals for a given stellar mass. In Figure 11, we also display the best-fit relations for a sample of SDSS ellipticals and spirals from Zhang & Yang (2019). Their relations agree well with those of Lange et al. (2015).

In Figure 11, we also overlay the Lange et al. (2016) best-fit lines for S0-Sa, Sab-Scd, and Sd-Irr galaxies for a sample of GAMA galaxies with $0.002 < z < 0.06$. All three morphological classes have similarly steep slopes of about 0.33, however, the y-intercept of the relation increases from early to late type (i.e., later type galaxies have larger effective radii for a given mass than earlier types). Our relation for multi-arm galaxies is flatter than their relations, but agrees well at the high mass end with that of Sab-Scd galaxies. Our grand design galaxies mostly lie between their relations for Sab-Scd and S0-Sa galaxies at the high mass end, but above their relation for Sab-Scd at the low mass end.

Our samples appear deficient in low mass, small size galaxies ($\log R50 < 0.04$ and $\log (M^*/M_\odot) < 9.5$) compared to the Lange et al. (2016) best-fit lines. This deficiency is not a consequence of how the half light radius was determined; using the NSA Sérsic half-light radius rather than the Petrosian radius shifts our relations to higher radii, making the offset even larger. One factor that may contribute to this deficiency is our selection criteria. For grand design galaxies we are limited to radii $\geq 7''$, due to our requirement that the spiral arms must be traced out at least $5''$ in the galaxy, starting at a radius of $2''$. Assuming a relatively low concentration of $C = 2$, and assuming that the arms extend out to R90, this means that R50 must be $\geq 3'5$. At a distance of $z = 0.02$, this corresponds to $R50 = 1.5$ kpc, or $\log R50 = 0.18$. Thus the bottom area on these plots is not accessible in our study for low redshift, low concentration galaxies. However, higher concentration galaxies could fall in this region.

However, the main reason for the flatter slopes for our samples in Figure 11 compared to the relations for S0-Sa, Sab-Scd, and Sc-Irr galaxies is the anti-correlation between TType and stellar mass (Figure 6). For both grand design and multi-armed galaxies, lower mass galaxies have later TTypes and smaller concentrations. Our low mass galaxies of both arm classes are close to the Lange et al. (2016) relation for late-type spirals because they have small concentrations, and preferentially are classified as late-type spirals. Both our grand design sample and our multi-armed sample lack low mass galaxies classified as type S0-Sb (Figure 6).

5.1.4. Pseudo-Bulges vs. Classical Bulges

Based on the criterion $\log \Delta\Sigma_1 > 0$ from Luo et al. (2020), 70% of our grand design galaxies host classical bulges, but only 50% of the multi-armed galaxies. The question of pseudo-bulges vs. classical bulges in grand design, multi-armed, and flocculent galaxies was addressed before by Bittner et al. (2017), by fitting Sérsic profiles to the bulges of their spiral galaxies. According to Kormendy & Kennicutt (2004) and Fisher & Drory (2008), pseudo-bulges and classical bulges

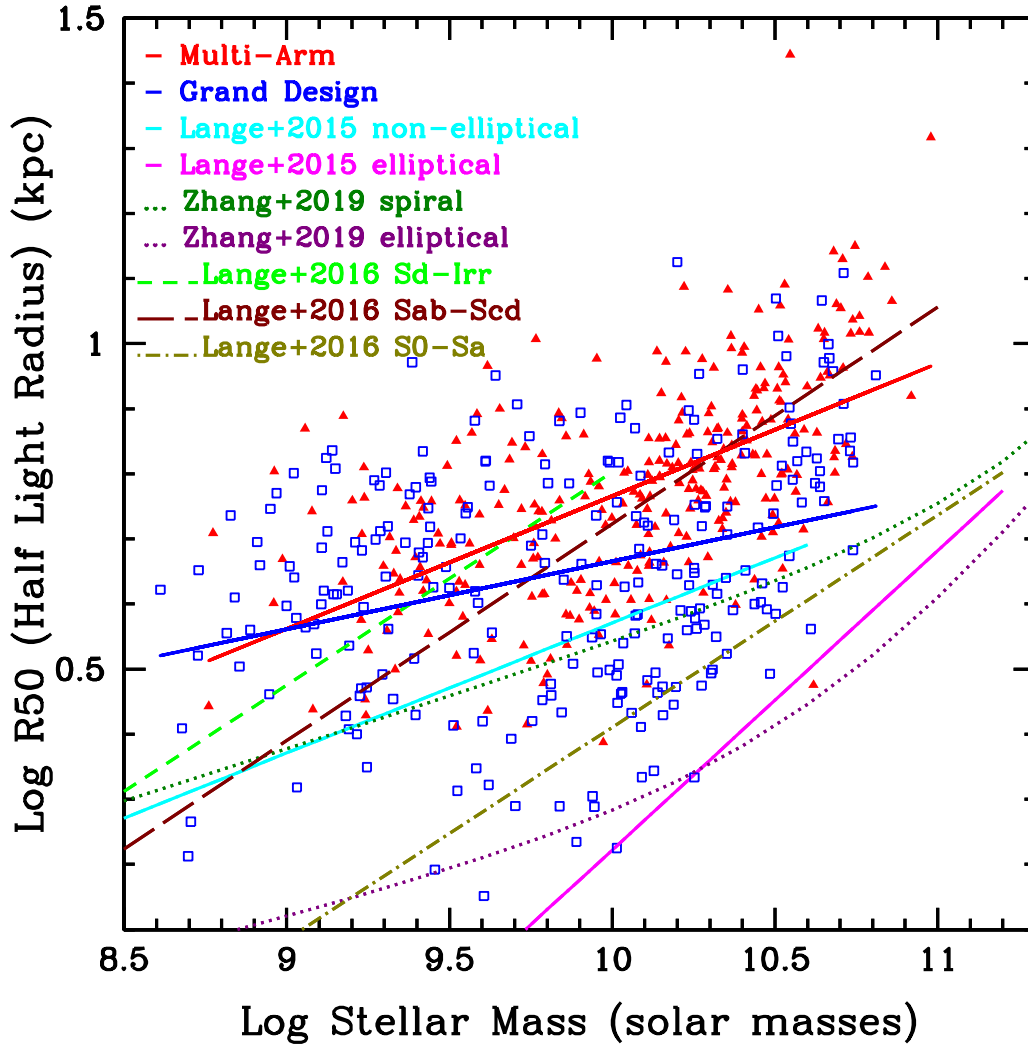


Figure 11. Plot of R50 vs. stellar mass for our multi-armed (red) vs. grand design galaxies (blue), as in Figure 5. Results from other studies are overlaid. See text for details.

can be distinguished by the bulge Sérsic index n ; $n < 2$ signals a pseudo-bulge, while $n > 2$ suggests a classical bulge. Bittner et al. (2017) found that the distributions of bulge Sérsic indices for grand design and multi-armed galaxies extend to high n , however, less than half of their galaxies have $n > 2$. They found similar distributions of bulge Sérsic indices for the grand design and multi-armed galaxies, implying similar numbers of classical vs. pseudo-bulges.

As noted earlier, our sample is skewed to higher stellar masses than the [Bittner et al. \(2017\)](#) sample. We might therefore expect to see higher fractions of classical bulges than the [Bittner et al. \(2017\)](#) study. The percentage of classical bulges is known to increase with increasing stellar mass. Classical bulges dominate above $\log(M^*/M_\odot) \sim 10.5$, while pseudo-bulges are more common at lower masses ([Sachdeva et al. 2020](#); [Hu et al. 2023](#)). The tendency of grand design galaxies to have earlier Hubble types and larger concentrations for a given mass may also favor classical bulges. Classical bulges are more frequent in early-type spirals, although they are seen in the full range of spiral Hubble types ([Kormendy & Kennicutt 2004](#); [Laurikainen et al. 2007](#)). Concentration is also weakly correlated with bulge Sérsic index, although concentration alone cannot be used to distinguish between pseudo-bulges and classical bulges ([Gadotti 2009](#)).

As an independent check on the nature of the bulges in the centers of our galaxies, we cross-correlated our list of galaxies with the [Domínguez Sánchez et al. \(2022\)](#) catalog of photometric parameters for MaNGA galaxies. Their catalog includes the results of fits to the SDSS surface brightness profiles of the galaxies. Following [Hu et al. \(2023\)](#), for this comparison we limited the sample to galaxies with a reliable 2-component fit (bulge plus disk) by setting the parameters FLAG_FIT=2 and FLAG_FAILED.SE=0, and requiring the half-light radius for the disk component to be larger than that for the bulge component and the half-light radius of the bulge to be larger than $0''.75$ (about the half width half maximum point spread function). A total of 41 and 32 of our multi-armed and grand design galaxies, respectively, meet these criteria. Of these, eight (20%) of the multi-armed and nine (28%) of the grand design have a bulge Sérsic index larger than 2. These percentages are smaller than those implied by the $\Delta\Sigma_1$ analysis, however, the sample sizes are small, and the uncertainties on the bulge Sérsic indices are sometimes quite large. A more detailed study of the radial light profiles in these galaxies using higher spatial resolution images would be helpful to further test the idea that grand design galaxies are more likely to host classical bulges.

5.1.5. *sSFR vs. Arm Counts*

We find no relation between arm count and sSFR, if one removes the effect of concentration (i.e., comparing galaxies with similar concentrations and stellar masses, we see no difference between the sSFRs of grand design and multi-armed galaxies.) This conclusion agrees with that of [Smith et al. \(2022a\)](#), who found that the $m=3$ Fourier amplitude of spiral galaxies is weakly correlated with sSFR, but when accounting for differences in concentration and stellar mass, no trend is present. We also see little difference in the sSFRs of multi-armed and grand design galaxies if we compare galaxies of similar stellar masses and similar central surface brightnesses.

There have been a number of GZ2 studies investigating how sSFR depends upon the number of spiral arms. Some studies concluded that 3-armed systems have higher sSFRs than 2-armed galaxies ([Hart et al. 2016](#); [Smith et al. 2022b](#)), other studies ([Willett et al. 2015](#); [Hart et al. 2017](#)) did not see a statistical difference in sSFR between galaxies with 2 arms and galaxies with 3 arms, and one study ([Porter-Temple et al. 2022](#)) concluded that multi-armed galaxies have lower sSFR. These different results might be a consequence of sample effects, since each study includes galaxies with different M^* ranges, and sSFR is a function of both M^* and concentration. The [Hart et al. \(2016\)](#) and [Smith et al. \(2022b\)](#) samples are limited to high mass galaxies ($\log(M^*/M_\odot) \geq 10.6$ and $10.25 \leq \log(M^*/M_\odot) < 10.75$, respectively). Within these mass ranges, when galaxies with all concentrations are included we find sSFRs that are significantly higher or marginally significantly higher for multi-armed galaxies than for grand design galaxies, consistent with their results. However, in this mass range there are significant differences between the concentrations of grand design and multi-armed galaxies (Table 1) and sSFR also depends upon concentration. When we remove the effect of concentration by comparing only galaxies with similar concentrations, the sSFRs of multi-armed galaxies are similar to those of grand design galaxies (Figure 8). We conclude that the differences in sSFR between 3-armed and 2-armed galaxies found by [Hart et al. \(2016\)](#) and [Smith et al. \(2022b\)](#) are a consequence of differences in concentration between the two sets of galaxies.

The [Porter-Temple et al. \(2022\)](#) GZ2 study includes galaxies with a wide range of stellar mass, so here we need to account for the effect of averaging over a range of masses. Their sample included galaxies with $9 \leq \log(M^*/M_\odot) < 11$, and was strongly biased towards lower mass galaxies. Since their 2-armed galaxies have lower masses on average than their 3+armed galaxies (in agreement with our results) and sSFR tends to decrease with increasing M^* (Figure 8), weighting over their mass distribution may cause their 2-armed galaxies to have higher sSFRs than the 3+armed galaxies on average.

In the Willett et al. (2015) and Hart et al. (2017) studies, the sSFR variation with M^* is investigated explicitly for 2-armed galaxies vs. 3+armed galaxies. They reach the same conclusion as we do, that the trend with M^* is independent of the number of arms.

5.2. Comparison with Theories of Spiral Arm Production and Maintenance

Statistical studies of galaxies with multi-armed vs. grand design patterns like the current study provides important constraints on theories of spiral arm formation and maintenance. In this section, we discuss the various models of spiral arm development in light of the data.

The sample of galaxies studied in the current paper contains very few strongly interacting pairs or cluster galaxies, so we cannot directly compare with earlier studies of interacting or cluster galaxies. A more detailed study of the environment around each galaxy in the current sample is beyond the scope of this study, and we leave that to future work. Ideally, since arm class is a function of both concentration and stellar mass, this study would be repeated with a large enough sample to allow separation into subsets based on M^* and C as well as environment. In any case, our observation that grand design galaxies are systematically offset from multi-armed galaxies in the concentration- M^* plane strongly suggests that the specific spiral pattern observed in a galaxy depends at least in part on the internal structure of the galaxy, and not just on external influences. Although gravitational interactions are clearly responsible for some spiral patterns, they are likely not the sole explanation for the difference between grand design and multi-armed galaxies.

We have not included an analysis of bars in the current sample of galaxies in this paper; that task is also left to future work. Past studies on the statistics of bars in spirals give ambiguous results. Although correlations are seen between bar strength and arm strength in spirals (Block et al. 2004; Buta et al. 2005; Yu & Ho 2020), it is unclear whether the bar causes the arms, or whether conditions that favor bar production also favor strong arms (Salo et al. 2010; Díaz-García et al. 2019). In any case, the presence of grand design spiral arms in unbarred isolated galaxies implies that another process is necessary for at least in some galaxies.

Observationally, we find that grand design galaxies are more likely to host classical bulges than multi-armed galaxies, and have larger concentrations for a given stellar mass. This suggests that the presence of a dense concentrated bulge aids the development and/or longevity of a 2-armed spiral pattern. This is consistent with the idea that a massive bulge may reflect a spiral wave and make it long-lived, as suggested by Bertin et al. (1989). In this scenario, a trailing spiral wave moving inwards reflects off of the high Q barrier caused by the bulge, and returns outwards as a weak leading wave to corotation, at which point swing amplification reverses it again (Mark 1976, 1977; Bertin et al. 1989). Under the right conditions, a long-lived spiral mode can be produced. The N-body simulations of Saha & Elmegreen (2016) appear to capture this process, as they produce a strong 2-armed spiral mode wave with a constant pattern speed that lasts 4 – 5 Gyrs.

The formation and evolution of large scale spirals in galaxies can be modeled in terms of ensembles of resonant eccentric orbits (Struck 2015, 2024, in prep). These orbit calculations show that it is easier to get 2-arm-supporting resonant eccentric orbits over a range of pattern speeds and radii when the rotation curve is falling or flat, as opposed to rising. In contrast, resonance eccentric orbits associated with $m=3$ and $m=4$ spirals are favored over a range of radii when the rotation curve is rising. This suggests that a centrally concentrated gravitational potential (associated with a flat or falling rotation curve) favors 2-armed spiral patterns, and a more extended mass distribution favors multi-armed structure. This is consistent with our observational results.

In contrast to the long-lived spiral waves in the Saha & Elmegreen (2016) simulations, simulations in which spirals are caused by instabilities in the disk enhanced by swing amplification produce transient and recurrent arms (Sellwood & Carlberg 1984; Sellwood 2000; Baba et al. 2009, 2013; D’Onghia et al. 2013; Michikoshi & Kokubo 2018). Although these simulations frequently produce multi-armed and flocculent structures, two-armed morphologies can also appear, especially when the disk is massive compared to the halo (D’Onghia 2015; Michikoshi & Kokubo 2018) and/or the shear rate is high (Michikoshi & Kokubo 2018). A falling rotation curve implies a high shear rate, thus these simulations show quantitative agreement with the orbit calculations of Struck (2024).

With simulations it is difficult to produce an unbarred 2-armed galaxy, since a massive disk tends to be unstable to bar formation (Efstathiou et al. 1982; Bottema 2003; Fujii et al. 2018), and a massive halo tends to suppress both bar formation and the formation of a 2-armed spiral (Sellwood et al. 2019; Sellwood & Carlberg 2023). A possible way to prevent bar formation is by adding a classical bulge (Sellwood 1985). Orbit calculations suggest that a centrally concentrated gravitational potential may not support very eccentric resonance orbits in their inner regions (Struck

2024), suggesting, in turn, that it is hard to form bars in such systems. In a recent set of simulations, Saha & Elmegreen (2018) were able to produce unbarred spiral patterns by including a compact and dense spherical classical bulge. This produces a strong inner Lindblad resonance (ILR) with a small radius, which inhibits the growth of a bar. The large ratio of random motions to ordered motion in the central region of the galaxy may stabilize the inner disk and prevent bar formation. More recently, Jang & Kim (2023) ran a series of simulations with a range of bulge/disk mass ratios and bulge and halo sizes. Some of these simulations produced spirals without bars; the barless models tend to have large masses within the inner 0.1 kpc relative to the disk mass. Most of the Jang & Kim (2023) simulations of unbarred spiral galaxies produce multi-armed spiral patterns, but a subset appear to have two dominant arms. The models with the two dominant arms have the largest bulge/disk mass ratios.

These models suggest that the number of arms in a galaxy is a function of the relative masses and sizes of the bulge, the disk, and the halo. Our observations show that the concentration and bulge properties of a galaxy play important roles in determining the number of arms present. Although we do not have direct evidence of long-lived wave modes operating in our sample of galaxies, the fact that grand design patterns are more common in galaxies with large bulges is suggestive, and supports the hypothesis that a large bulge favors the production of two-armed spirals, or increases their longevity.

More work on the topic of arm count vs. galaxy structure is needed on both the theoretical and the observational side. Large statistical studies of the rotation curves of spirals with different arm morphologies would better determine how the arm morphology relates to halo, disk, and bulge mass distributions in galaxies. Future studies of arm morphology as a function of stellar mass, concentration, Hubble Type, and rotation curve may provide clues to the merger and star formation histories of galaxies. Combining the known relation between stellar mass and the ratio of stellar mass to halo mass (Behroozi et al. 2013; Mandelbaum et al. 2006) with observed trends in the grand design vs. multi-arm fraction with stellar mass, concentration, and TType may also help constrain galaxy evolution models.

Above stellar masses of $\sim 10^{10} M_{\odot}$, a marked increase in the number of spirals with high concentrations has been observed, producing a ‘bend’ in the concentration- M^* diagram for spirals (Luo et al. 2020; Smith et al. 2022a). This bend is shown in our Figure 4, where the scatter in C increases at higher M^* . Luo et al. (2020) suggest that this bend is caused by the growth of classical bulges. Our current study shows that the high C , high M^* spirals above this bend tend to have grand design patterns. Below the bend, grand design galaxies tend to have lower observed concentrations (though still larger than those of multi-armed galaxies of the same stellar mass). Combined with a better theoretical understanding of the origins of grand design galaxies, these observations may provide clues to how galactic bulges evolve over time. In the Hubble Deep Field, few grand design galaxies are seen at $z = 1$ compared to the local Universe (van den Bergh et al. 1996). This result may be a consequence of bulge growth with time. More work is needed on how the fraction of grand design vs. multi-armed galaxies varies with redshift.

6. SUMMARY

We developed a method to use Galaxy Zoo 3D spiral arm masks to distinguish multi-armed galaxies from grand design spirals, and created a catalog of 299 multi-armed galaxies and 245 grand design systems. We found reasonable agreement between our classifications and arm counts from GZ2 and published normalized $m=3$ Fourier amplitudes.

Galaxies classified as grand design are offset in the concentration- M^* plane relative to multi-armed galaxies, with larger concentrations and smaller stellar masses on average. Grand design galaxies also tend to have earlier Hubble types than multi-armed galaxies, with the relation skewing to later types at lower stellar masses. The grand design and multi-armed galaxies have similar $R90$ sizes for a given stellar mass, but the grand design galaxies have smaller half-light radii. The larger concentrations seen in grand design galaxies are due to an excess of light in the central region, rather than larger overall sizes. When comparing multi-armed and grand design galaxies with similar masses and concentrations, they have similar sSFRs. Based on the central surface mass densities in these galaxies, we conclude that grand design galaxies are more likely to host classical bulges, while multi-armed galaxies are more likely to have pseudo-bulges.

Our observations are consistent with theoretical models in which dense classical bulges favor the development and possibly the longevity of two-armed spiral patterns. Although other mechanisms, such as interactions and bars, may also produce grand design spirals, the strong relation between arm class and concentration implies that the internal structure of a galaxy is a dominant factor in determining the number of arms.

Acknowledgments

This research was supported by a grant from the NASA Tennessee Space Grant consortium. We thank the anonymous referee for valuable suggestions that greatly improved this paper. We also thank Si-Yue Yu and Bruce Elmegreen for helpful comments on this manuscript. We greatly appreciate the work of the Galaxy Zoo-3D team and the GZ-3D volunteers who made this project possible. This publication uses data generated via the Zooniverse.org platform, development of which is funded by generous support, including a Global Impact Award from Google, and by a grant from the Alfred P. Sloan Foundation. This research also made use of the VizieR catalogue access tool and the cross-match service at the Centre de Données Astronomiques de Stasbourg, CDS, Strasbourg, France. This research has also made use of the NASA/IPAC Extragalactic Database (NED), which is operated by the Jet Propulsion Laboratory, California Institute of Technology, under contract with the National Aeronautics and Space Administration. This research is based in part on data from the Sloan Digital Sky Survey. Funding for the Sloan Digital Sky Survey IV has been provided by the Alfred P. Sloan Foundation, the U.S. Department of Energy Office of Science, and the Participating Institutions. SDSS-IV acknowledges support and resources from the Center for High-Performance Computing at the University of Utah. The SDSS web site is www.sdss.org. SDSS-IV is managed by the Astrophysical Research Consortium for the Participating Institutions of the SDSS Collaboration including the Brazilian Participation Group, the Carnegie Institution for Science, Carnegie Mellon University, the Chilean Participation Group, the French Participation Group, Harvard-Smithsonian Center for Astrophysics, Instituto de Astrofísica de Canarias, The Johns Hopkins University, Kavli Institute for the Physics and Mathematics of the Universe (IPMU) / University of Tokyo, the Korean Participation Group, Lawrence Berkeley National Laboratory, Leibniz Institut für Astrophysik Potsdam (AIP), Max-Planck-Institut für Astronomie (MPIA Heidelberg), Max-Planck-Institut für Astrophysik (MPA Garching), Max-Planck-Institut für Extraterrestrische Physik (MPE), National Astronomical Observatories of China, New Mexico State University, New York University, University of Notre Dame, Observatório Nacional / MCTI, The Ohio State University, Pennsylvania State University, Shanghai Astronomical Observatory, United Kingdom Participation Group, Universidad Nacional Autónoma de México, University of Arizona, University of Colorado Boulder, University of Oxford, University of Portsmouth, University of Utah, University of Virginia, University of Washington, University of Wisconsin, Vanderbilt University, and Yale University.

APPENDIX

A. EXAMPLE GZ-3D MASKS AND SDSS IMAGES

In Figure 12, we provide examples of galaxies in our final vetted sample of grand design galaxies. Example galaxies from our final sample of multi-armed galaxies are shown in Figure 13. In these figures, we provide both the GZ-3D mask of the galaxy and the SDSS g image. On the GZ-3D masks, we have overlaid contours in green which mark the levels of one and three counts. We have also overlaid ellipses marking the inner and outer radii of the largest radial range in which our code counts two arms (for the grand design galaxies) or three arms (for the multi-armed galaxies).

B. POSSIBLE SELECTION EFFECTS

In this section, we investigate some possible biases in our sample, and test whether these selection effects affect the conclusions of this paper.

B.1. *The Limited Field of View*

Our arm-tracing method is limited by the $52'' \times 52''$ GZ-3D field of view. This means that we are not able to measure arms out very far in nearby galaxies. In the left panel of Figure 14, we provide a plot of the maximum radial distance to which we measure arms, $R(\text{max})$, vs. $R(\text{edge})$, the radius to the edge of the observed field of view, for all of the galaxies in the low z GZ-3D sample. $R(\text{max})$ is defined as the maximum radial extent of an arm above our threshold = 3 cutoff in the GZ-3D masks. $R(\text{edge})$ in kpc is proportional to redshift, which is marked on the top axes of these plots. The distributions of galaxies we identify as multi-armed (red open triangles) is similar to that of the grand design galaxies (blue open squares). In this plot, we also identify galaxies with NSA $R90$ sizes that are greater than $1.2 \times R(\text{edge})$. These are galaxies with large physical radii compared to the field of view, and so are more likely to have arms that are truncated by the field of view. The series of datapoints marking the one-to-one relation which

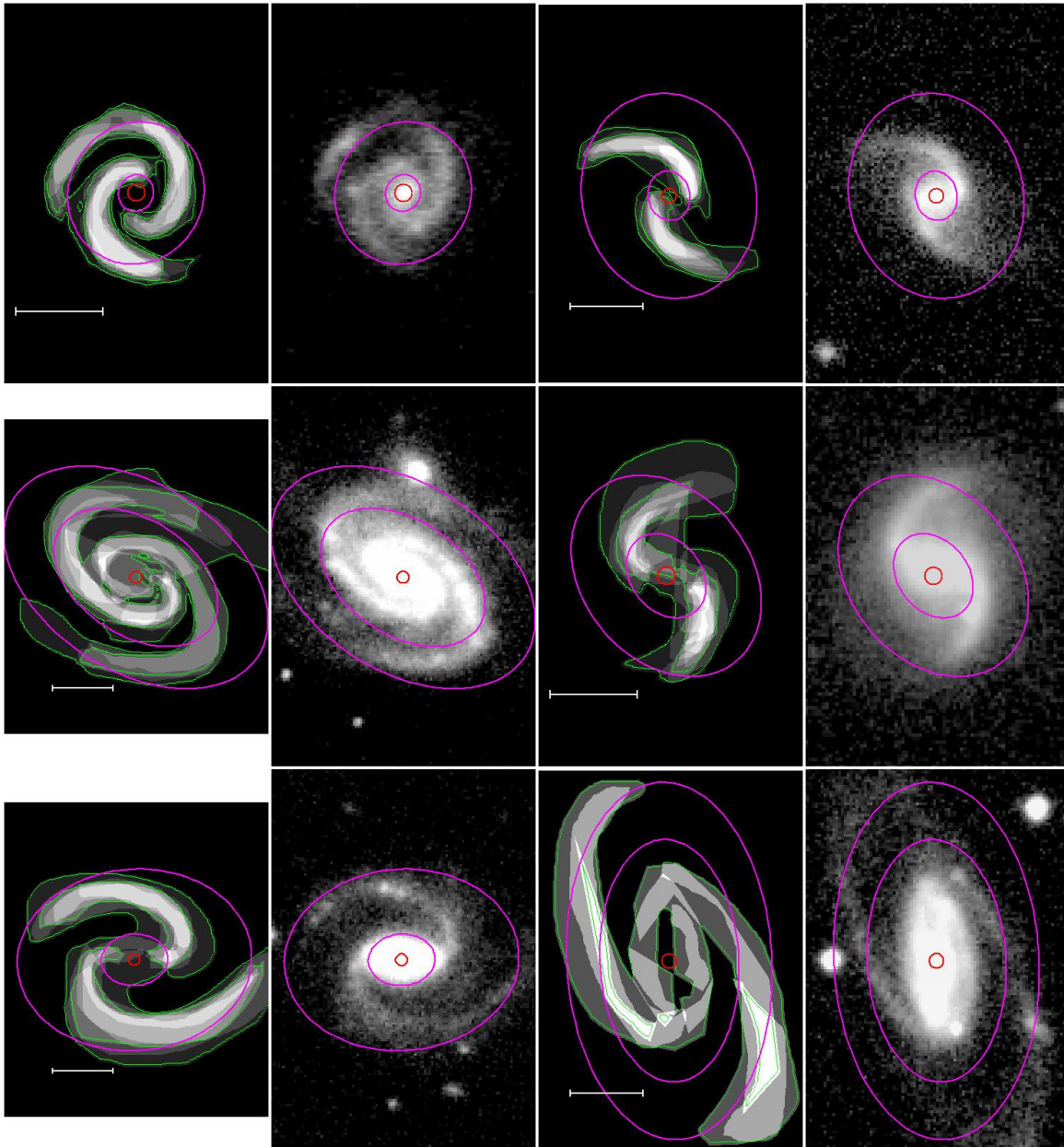


Figure 12. Examples of six galaxies identified by the code as grand design and confirmed by eye. The first picture of each galaxy is the GZ-3D mask; the second picture is the SDSS g-image. The two green contours on the GZ-3D masks correspond to 1 and 3 counts. The magenta ellipses show the inner and outer radii of the largest continuous radial range marked as 2-armed by our software. The red circle indicates the center of the galaxy as marked by GZ-3D participants. On the SDSS g-band images, the same circle and ellipses overlaid. In order left to right, top to bottom, the galaxies are: MaNGA ID 1-1811 = IAU J101927.42-000204.3; MaNGA ID 1-32942 = IAU J010650.99-003413.7; MaNGA ID 1-260943 = IAU J141031.43+385353.8; MaNGA ID 1-555127 = IAU J023421.64-075224.2; MaNGA ID 1-567320 = IAU J094120.45+211656.9; MaNGA ID 1-605134 = IAU J081752.00+125350.9. The white scale bars are $10''$.

bisects these plots marks the maximum distance we are able to measure arms. We are able to trace arms to greater extents in more distant galaxies, and therefore our arm measurements may be artificially truncated for nearby and/or physically large galaxies. This potentially causes a redshift bias in our study, in that our method of counting arms and flagging galaxies searches an increasingly large fraction of the galaxian disk at increasing redshift.

In the right panel of Figure 14, we provide histograms of $R(\text{max})$, the maximum radius in kpc out to which we identify spiral arms. There is a large spread in $R(\text{max})$ for the galaxies in the sample, from 2 kpc to 25 kpc. Although

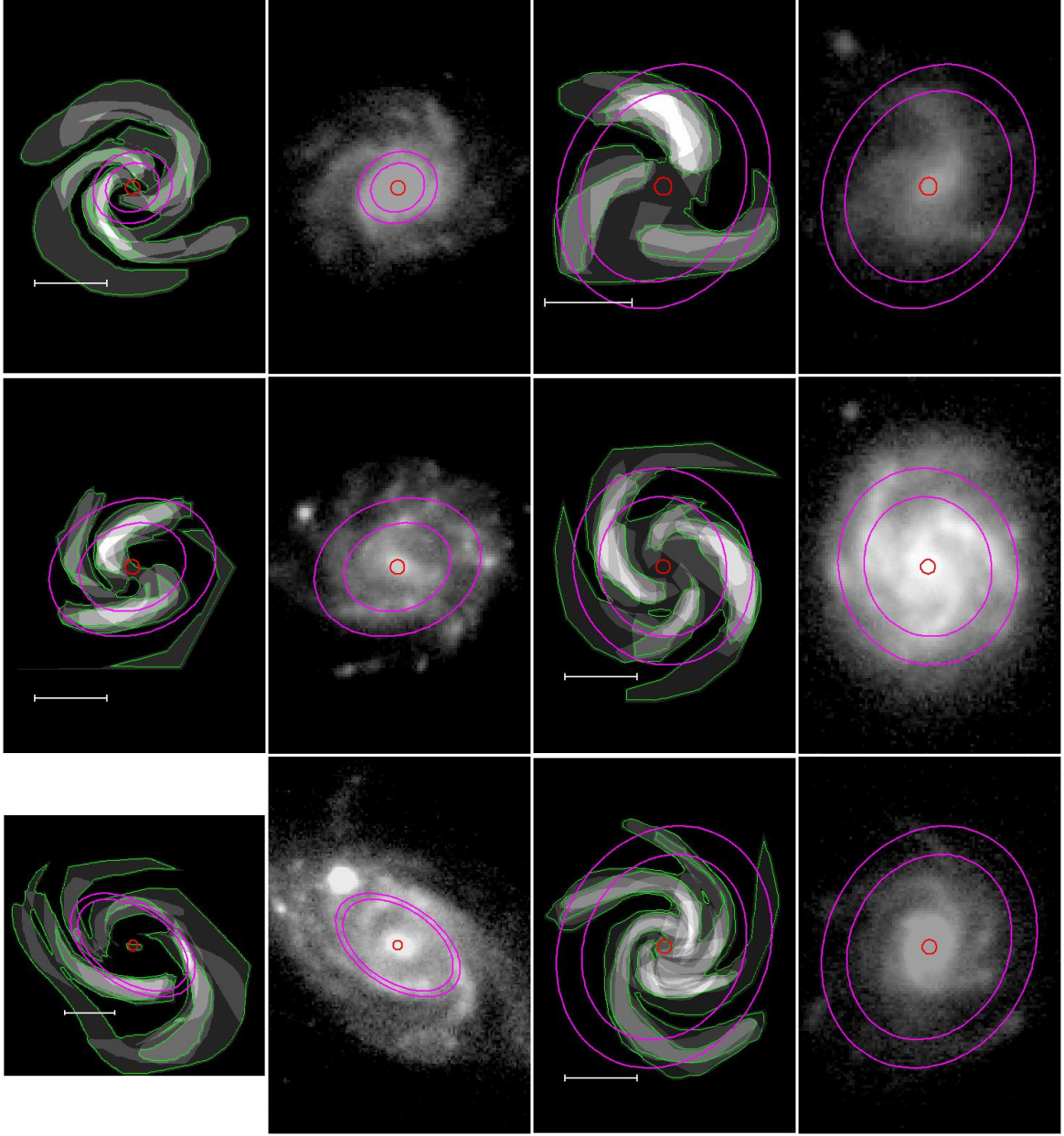


Figure 13. Examples of six galaxies identified by the code as multi-armed and confirmed by eye. The first picture of each galaxy is the GZ-3D mask; the second picture is the SDSS g-image. The two green contours on the GZ-3D masks correspond to 1 and 3 counts. The magenta ellipses show the inner and outer radii of the largest continuous radial range marked as 3-armed by our software. The red circle indicates the center of the galaxy as marked by GZ-3D participants. On the SDSS g-band images, the same circle and ellipses overlaid. In order left to right, top to bottom, the galaxies are: MaNGA ID 1-30797 = IAU J001039.34-000310.3; MaNGA ID 1-104906 = IAU J014636.04-085944.3; MaNGA ID 1-397480 = IAU J124727.84+403359.6; MaNGA ID 1-604111 = IAU J033758.99-061611.9; MaNGA ID 1-638560 = IAU J121744.69+131029.9. The white scale bars are $10''$.

the peak in the histogram of $R(\max)$ is slightly lower for grand design galaxies than for multi-armed galaxies, there is only a marginal statistical difference between the two samples (KS probability = 0.038). Dividing the sample up into narrow bins of M^* (0.3 dex bins), we see an increase in $R(\max)$ with M^* , but within a given M^* bin KS tests do not show a significant difference between grand design and multi-armed galaxies.

In the left panel of Figure 15, we plot $R(\max)$ normalized by the R_{90} radius. The peak of the distribution of $R(\max)/R_{90}$ for the grand design galaxies is lower than for the multi-armed galaxies. A KS test shows a significant

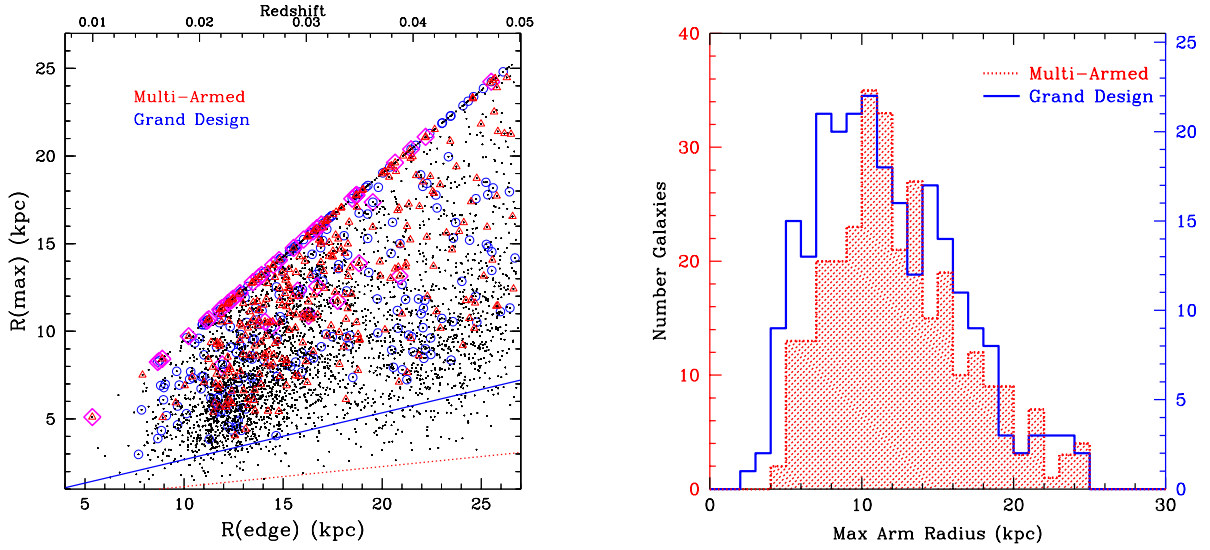


Figure 14. Left: Plot of $R(\text{max})$, the maximum distance out to which we trace spiral arms, vs. $R(\text{edge})$, the edge of the GZ-3D field of view. The small black dots are all of the galaxies in the $z < 0.05$ GZ-3D sample for which we are able to mark spiral arms. Red open triangles mark the galaxies that we classified as multi-armed. Blue open circles are galaxies classified as grand design. Magenta open diamonds mark galaxies which have $R_{90}/R(\text{edge}) > 1.2$. These are galaxies that are physically large compared to the GZ-3D field of view. The red dotted line is the minimum $R(\text{max})$ possible for galaxies flagged as 3-armed. The blue solid line is the minimum $R(\text{max})$ possible for a galaxy defined as grand design by our definition. Right: Histograms of the maximum radius out to which we are able to reliably mark spiral arms (i.e., at a threshold = 3) for the multi-armed galaxies (red hatched histogram) and the grand design galaxies (blue).

difference for the full M^* range (KS probability 0.00048). Sub-dividing into small mass bins, significant differences are present for the $10 \leq \log(M^*/M_\odot) < 10.3$ and $10.3 \leq \log(M^*/M_\odot) < 10.6$ bins (KS probabilities of 0.00013 and 0.00375, respectively), with the grand design galaxies having larger ratios. The grand design galaxies in these bins have median $R(\text{max})/R_{90}$ values larger than one (1.10 and 1.11, respectively). The GZ-3D participants were able to trace the spiral arms out to large distances in the grand design galaxies. Why there is this difference between grand design and multi-armed galaxies is uncertain. One possibility is that the arms are stronger and more distinct in grand design galaxies, making them easier to see further out in the galaxies. However, we don't see a significant difference in arm strengths between grand design and multi-armed galaxies (Figure 9).

To investigate possible selection effects due to spiral arms extending beyond the edge of the field of view, we re-ran the KS tests comparing stellar mass, concentration, and sSFR for the two samples of galaxies, after eliminating galaxies with $R(\text{max}) \geq 0.95 R(\text{edge})$ (i.e., galaxies that may have truncated arms in GZ-3D). The differences in stellar mass and concentration between grand design and multi-armed galaxies persist, indicating that these differences are not caused by selection effects from the limited field of view. We do not see significant differences in the sSFRs of the grand design and multi-armed galaxies when binning by C and M^* as in Figure 8, after eliminating galaxies with $R(\text{max}) \geq 0.95 R(\text{edge})$. Thus our basic conclusions about M^* , C , and sSFR do not change when eliminating galaxies that may have arms that are truncated by the limited field of view.

B.2. Inclination

We also checked to see if the inclination of the galaxy (i.e., the ellipticity of the SDSS image) biases our classification into grand design vs. multi-armed. In the right panel of Figure 15, we provide histograms of the NSA ellipticity of our multi-armed and grand design galaxies. There is a clear difference, with the galaxies classified as multi-armed having

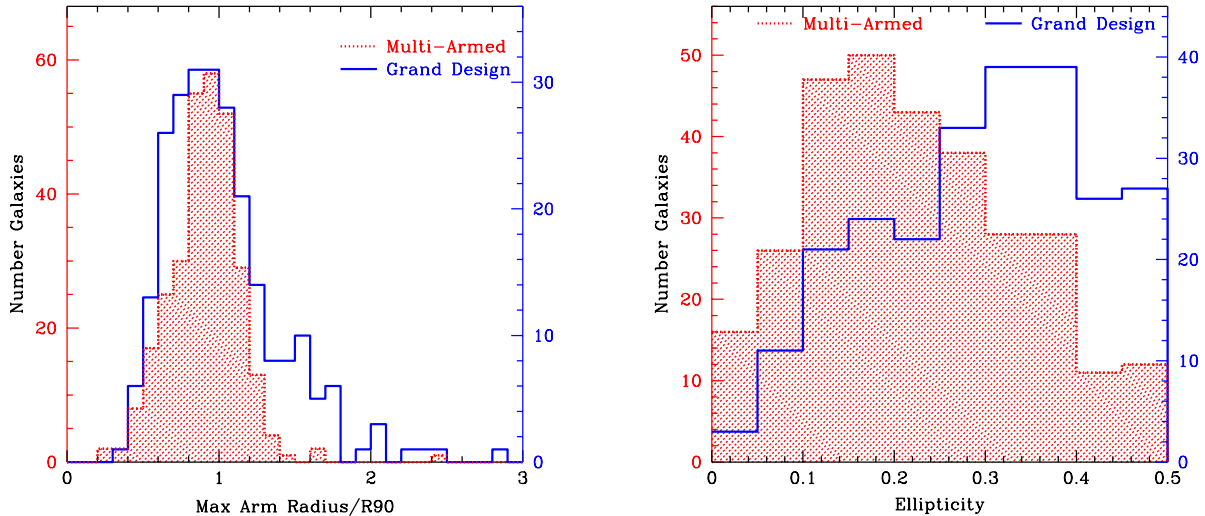


Figure 15. left: Histograms of $R(\max)$ divided by $R90$, where $R90$ is the radius enclosing 90% of the light. Right: histograms of the NSA ellipticities for the multi-armed galaxies (red hatched) and grand design galaxies (blue).

smaller ellipticities than the grand design galaxy. In other words, the multi-armed galaxies in our sample are more face-on on average than the grand design galaxies. This result is confirmed by a KS test (KS probability 10^{-10}).

The reason for the observed difference between the two samples is uncertain. It may be harder to see all of the arms if the galaxy is inclined, which may cause viewers to sometimes miss arms, leading to an undercount of the arms in multi-armed galaxies. Viewers may also be more likely to not to mark any arms at all in inclined galaxies, causing the galaxy not to be included in our final sample. Another possibility is that the ellipticity of a galaxy as determined from the outer optical isophotes may be over-estimated for galaxies with two dominant strong arms.

To test whether this difference in inclination between the two samples is responsible for the observed differences in M^* and C between the two samples and the lack of an observed difference in sSFR, we re-ran the KS tests for M^* , C , and sSFR, limiting the sample to only the most face-on galaxies (ellipticity < 0.25). The main results still hold with these face-on sub-samples. The only difference is that, when the ellipticity is restricted to < 0.25 , no significant differences in concentration between grand design and multi-armed galaxies are seen for the $9.4 \leq \log(M^*/M_\odot) < 9.7$ bin. A difference in concentration is still present in the higher mass bins. No differences in sSFR are seen between the two groups after the galaxies are binned in both C and M^* , even after limiting the sample to galaxies with ellipticity < 0.25 .

B.3. Incompleteness

Our method of identifying multi-armed and grand design galaxies is quite incomplete; only $\sim 12\%$ of the original sample of 4449 $z < 0.05$, ellipticity ≤ 0.5 GZ-3D spiral arm galaxies end up in either of the final classes. In the left panel of Figure 16, we plot the fraction of galaxies in our original GZ-3D sample that were identified in this study as multi-armed and as grand design, as a function of concentration. At low concentrations, the multi-armed galaxies are a larger fraction of the total $z < 0.05$ population of GZ-3D galaxies. In the middle of the concentration range, the fractions that are grand design galaxies are higher. At all concentrations, however, only a small fraction of galaxies ended up in either of our final sample. The incompleteness is particularly high at large C .

For the galaxies in our original low z GZ-3D sample that have TTypes from Domínguez Sánchez et al. (2018), in the right panel of Figure 16 we plot the fraction of galaxies identified in this study as multi-armed or grand design, as a

function of TType. There is a clear difference between the multi-armed and grand design galaxies in this plot, with the grand design galaxies skewed to earlier TTypes. However, only a small fraction of the galaxies classified as $1 \leq \text{TType} < 7$ ended up in either our grand design or multi-armed sample. The incompleteness is highest at TType = 7 and TType = 1.

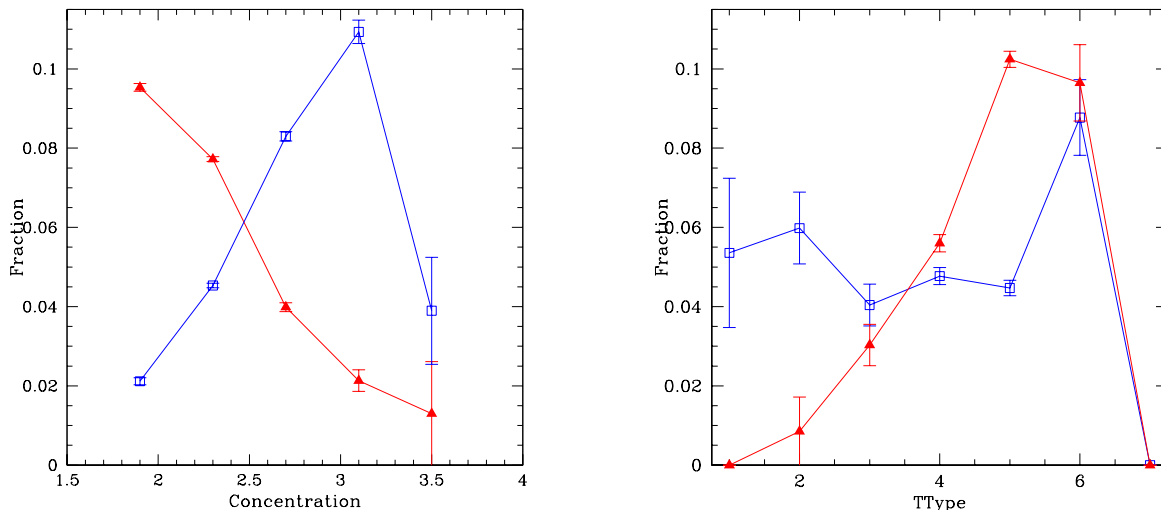


Figure 16. The fraction of the $z < 0.05$ GZ-3D galaxies in our final samples of multi-armed galaxies (red filled triangles) and grand design galaxies (blue open squares), as a function of concentration (left panel) and TType (right panel). The uncertainties are \sqrt{N} .

In the left panel of Figure 17, we plot the fraction of the original low z GZ-3D sample as a function of M^* . Except for the lowest mass bin, $9.1 \leq \log(M^*/M_\odot) < 9.4$, there are more multi-armed galaxies than grand design. The ratio of multi-armed to grand design is highest at $10.3 \leq \log(M^*/M_\odot) < 10.6$. The sample is more complete at higher masses. The right panel of Figure 17 displays completeness vs. ellipticity for the two classes of spirals. As noted earlier, there is a bias in that our multi-armed galaxies appear more face-on than the grand design galaxies.

Several factors may contribute to the observed incompleteness. First, insufficient resolution and/or sensitivity in the SDSS images of some galaxies may have caused the GZ-3D viewers to not mark the spiral arms, or to mark the arms incorrectly. Second, although the MaNGA GZ-3D sample was selected to avoid flocculent galaxies, some galaxies may have too short or too fragmented arms to be marked by the GZ-3D participants, or the spiral segments marked by the GZ-3D participants may be too short to meet our criteria for flagging. Third, in some cases the arms may have been hard to pick out in the images, having high pitch angles and/or low arm/interarm contrast. Fourth, some galaxies may not fit cleanly into either class. For example, some galaxies may be too peculiar and/or strongly interacting. Fifth, some GZ-3D viewers may have only marked two arms per galaxy, and may not have marked branches. This may cause multi-armed galaxies to end up in our grand design sample, and then be eliminated by the by-eye inspection.

To better understand the evolutionary relationship between grand design and multi-armed galaxies, it would be useful to determine the arm structures of all of the galaxies in the full $z < 0.05$ GZ-3D sample. Obtaining clear morphological information for a more complete sample of spirals will help us better understand the cause and evolution of spiral patterns in galaxies. In the future, it would be worthwhile repeating the current study with higher resolution, more sensitive images from more modern surveys such as the Dark Energy Survey or the Euclid telescope.

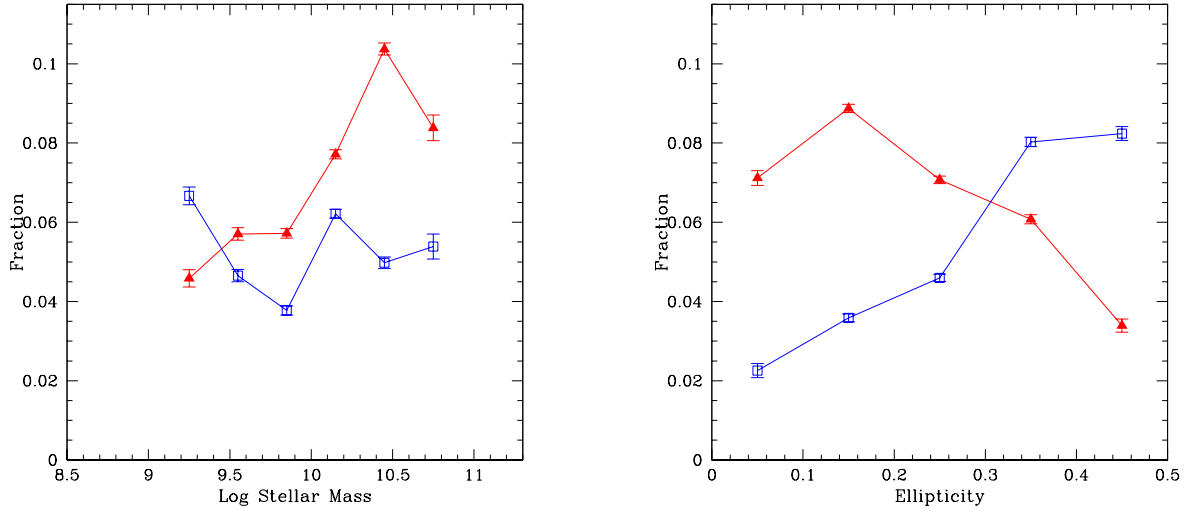


Figure 17. The fraction of the $z < 0.05$ GZ-3D galaxies in our final samples of multi-armed galaxies (red filled triangles) and grand design galaxies (blue open squares), as a function of stellar mass (left) and ellipticity (right). The uncertainties are \sqrt{N} .

REFERENCES

- Ann, H. B., & Lee, H.-R. 2013, *Journal of Korean Astronomical Society*, 46, 141, doi: [10.5303/JKAS.2013.46.3.141](https://doi.org/10.5303/JKAS.2013.46.3.141)
- Athanassoula, E. 1980, *A&A*, 88, 184
- Baba, J., Asaki, Y., Makino, J., et al. 2009, *ApJ*, 706, 471, doi: [10.1088/0004-637X/706/1/471](https://doi.org/10.1088/0004-637X/706/1/471)
- Baba, J., Saitoh, T. R., & Wada, K. 2013, *ApJ*, 763, 46, doi: [10.1088/0004-637X/763/1/46](https://doi.org/10.1088/0004-637X/763/1/46)
- Behroozi, P. S., Wechsler, R. H., & Conroy, C. 2013, *ApJ*, 770, 57, doi: [10.1088/0004-637X/770/1/57](https://doi.org/10.1088/0004-637X/770/1/57)
- Bertin, G., Lin, C. C., Lowe, S. A., & Thurstans, R. P. 1989, *ApJ*, 338, 104, doi: [10.1086/167183](https://doi.org/10.1086/167183)
- Bittner, A., Gadotti, D. A., Elmegreen, B. G., et al. 2017, *MNRAS*, 471, 1070, doi: [10.1093/mnras/stx1646](https://doi.org/10.1093/mnras/stx1646)
- Block, D. L., Buta, R., Knapen, J. H., et al. 2004, *AJ*, 128, 183, doi: [10.1086/421362](https://doi.org/10.1086/421362)
- Bottema, R. 2003, *MNRAS*, 344, 358, doi: [10.1046/j.1365-8711.2003.06613.x](https://doi.org/10.1046/j.1365-8711.2003.06613.x)
- Buta, R., Vasylyev, S., Salo, H., & Laurikainen, E. 2005, *AJ*, 130, 506, doi: [10.1086/431251](https://doi.org/10.1086/431251)
- Buta, R. J., Sheth, K., Athanassoula, E., et al. 2015, *ApJS*, 217, 32, doi: [10.1088/0067-0049/217/2/32](https://doi.org/10.1088/0067-0049/217/2/32)
- Byrd, G. G., & Howard, S. 1992, *AJ*, 103, 1089, doi: [10.1086/116128](https://doi.org/10.1086/116128)
- Carlberg, R. G., & Freedman, W. L. 1985, *ApJ*, 298, 486, doi: [10.1086/163634](https://doi.org/10.1086/163634)
- Choi, I. Y.-G., & Ann, H. B. 2011, *Journal of Korean Astronomical Society*, 44, 161, doi: [10.5303/JKAS.2011.44.5.161](https://doi.org/10.5303/JKAS.2011.44.5.161)
- Díaz-García, S., Salo, H., Knapen, J. H., & Herrera-Endoqui, M. 2019, *A&A*, 631, A94, doi: [10.1051/0004-6361/201936000](https://doi.org/10.1051/0004-6361/201936000)
- Dobbs, C., & Baba, J. 2014, *PASA*, 31, e035, doi: [10.1017/pasa.2014.31](https://doi.org/10.1017/pasa.2014.31)
- Dobbs, C. L., Pettitt, A. R., Corbelli, E., & Pringle, J. E. 2018, *MNRAS*, 478, 3793, doi: [10.1093/mnras/sty1231](https://doi.org/10.1093/mnras/sty1231)
- Dobbs, C. L., Theis, C., Pringle, J. E., & Bate, M. R. 2010, *MNRAS*, 403, 625, doi: [10.1111/j.1365-2966.2009.16161.x](https://doi.org/10.1111/j.1365-2966.2009.16161.x)
- Domínguez Sánchez, H., Huertas-Company, M., Bernardi, M., Tuccillo, D., & Fischer, J. L. 2018, *MNRAS*, 476, 3661, doi: [10.1093/mnras/sty338](https://doi.org/10.1093/mnras/sty338)
- Domínguez Sánchez, H., Margalef, B., Bernardi, M., & Huertas-Company, M. 2022, *MNRAS*, 509, 4024, doi: [10.1093/mnras/stab3089](https://doi.org/10.1093/mnras/stab3089)
- D’Onghia, E. 2015, *ApJL*, 808, L8, doi: [10.1088/2041-8205/808/1/L8](https://doi.org/10.1088/2041-8205/808/1/L8)
- D’Onghia, E., Vogelsberger, M., & Hernquist, L. 2013, *ApJ*, 766, 34, doi: [10.1088/0004-637X/766/1/34](https://doi.org/10.1088/0004-637X/766/1/34)

- Efstathiou, G., Lake, G., & Negroponte, J. 1982, *MNRAS*, 199, 1069, doi: [10.1093/mnras/199.4.1069](https://doi.org/10.1093/mnras/199.4.1069)
- Elmegreen, D. M. 1981, *ApJS*, 47, 229, doi: [10.1086/190757](https://doi.org/10.1086/190757)
- Elmegreen, D. M., & Elmegreen, B. G. 1982, *MNRAS*, 201, 1021, doi: [10.1093/mnras/201.4.1021](https://doi.org/10.1093/mnras/201.4.1021)
- . 1984, *ApJS*, 54, 127, doi: [10.1086/190922](https://doi.org/10.1086/190922)
- . 1987, *ApJ*, 314, 3, doi: [10.1086/165034](https://doi.org/10.1086/165034)
- Elmegreen, D. M., Elmegreen, B. G., & Dressler, A. 1982, *MNRAS*, 201, 1035, doi: [10.1093/mnras/201.4.1035](https://doi.org/10.1093/mnras/201.4.1035)
- Elmegreen, D. M., Elmegreen, B. G., Yau, A., et al. 2011, *ApJ*, 737, 32, doi: [10.1088/0004-637X/737/1/32](https://doi.org/10.1088/0004-637X/737/1/32)
- Fisher, D. B., & Drory, N. 2008, *AJ*, 136, 773, doi: [10.1088/0004-6256/136/2/773](https://doi.org/10.1088/0004-6256/136/2/773)
- Fujii, M. S., Bédorf, J., Baba, J., & Portegies Zwart, S. 2018, *MNRAS*, 477, 1451, doi: [10.1093/mnras/sty711](https://doi.org/10.1093/mnras/sty711)
- Gadotti, D. A. 2009, *MNRAS*, 393, 1531, doi: [10.1111/j.1365-2966.2008.14257.x](https://doi.org/10.1111/j.1365-2966.2008.14257.x)
- Goldreich, P., & Lynden-Bell, D. 1965, *MNRAS*, 130, 125, doi: [10.1093/mnras/130.2.125](https://doi.org/10.1093/mnras/130.2.125)
- Hart, R. E., Bamford, S. P., Casteels, K. R. V., et al. 2017, *MNRAS*, 468, 1850, doi: [10.1093/mnras/stx581](https://doi.org/10.1093/mnras/stx581)
- Hart, R. E., Bamford, S. P., Keel, W. C., et al. 2018, *MNRAS*, 478, 932, doi: [10.1093/mnras/sty1201](https://doi.org/10.1093/mnras/sty1201)
- Hart, R. E., Bamford, S. P., Willett, K. W., et al. 2016, *MNRAS*, 461, 3663, doi: [10.1093/mnras/stw1588](https://doi.org/10.1093/mnras/stw1588)
- Hu, J., wang, L., Ge, J., Zhu, K., & Zeng, G. 2023, arXiv e-prints, arXiv:2312.02721, doi: [10.48550/arXiv.2312.02721](https://doi.org/10.48550/arXiv.2312.02721)
- Hubble, E. P. 1926, *ApJ*, 64, 321, doi: [10.1086/143018](https://doi.org/10.1086/143018)
- Jang, D., & Kim, W.-T. 2023, *ApJ*, 942, 106, doi: [10.3847/1538-4357/aca7bc](https://doi.org/10.3847/1538-4357/aca7bc)
- Julian, W. H., & Toomre, A. 1966, *ApJ*, 146, 810, doi: [10.1086/148957](https://doi.org/10.1086/148957)
- Kauffmann, G., White, S. D. M., Heckman, T. M., et al. 2004, *MNRAS*, 353, 713, doi: [10.1111/j.1365-2966.2004.08117.x](https://doi.org/10.1111/j.1365-2966.2004.08117.x)
- Kormendy, J., & Kennicutt, Robert C., J. 2004, *ARA&A*, 42, 603, doi: [10.1146/annurev.astro.42.053102.134024](https://doi.org/10.1146/annurev.astro.42.053102.134024)
- Kormendy, J., & Norman, C. A. 1979, *ApJ*, 233, 539, doi: [10.1086/157414](https://doi.org/10.1086/157414)
- Lange, R., Driver, S. P., Robotham, A. S. G., et al. 2015, *MNRAS*, 447, 2603, doi: [10.1093/mnras/stu2467](https://doi.org/10.1093/mnras/stu2467)
- Lange, R., Moffett, A. J., Driver, S. P., et al. 2016, *MNRAS*, 462, 1470, doi: [10.1093/mnras/stw1495](https://doi.org/10.1093/mnras/stw1495)
- Laurikainen, E., Salo, H., Buta, R., & Knapen, J. H. 2007, *MNRAS*, 381, 401, doi: [10.1111/j.1365-2966.2007.12299.x](https://doi.org/10.1111/j.1365-2966.2007.12299.x)
- Lim, S. H., Mo, H. J., Lu, Y., Wang, H., & Yang, X. 2017, *MNRAS*, 470, 2982, doi: [10.1093/mnras/stx1462](https://doi.org/10.1093/mnras/stx1462)
- Lin, C. C., & Bertin, G. 1985, in *The Milky Way Galaxy*, ed. H. van Woerden, R. J. Allen, & W. B. Burton, Vol. 106, 513–530
- Lin, C. C., & Shu, F. H. 1964, *ApJ*, 140, 646, doi: [10.1086/147955](https://doi.org/10.1086/147955)
- . 1966, *Proceedings of the National Academy of Science*, 55, 229, doi: [10.1073/pnas.55.2.229](https://doi.org/10.1073/pnas.55.2.229)
- Luo, Y., Faber, S. M., Rodríguez-Puebla, A., et al. 2020, *MNRAS*, 493, 1686, doi: [10.1093/mnras/staa328](https://doi.org/10.1093/mnras/staa328)
- Mandelbaum, R., Seljak, U., Kauffmann, G., Hirata, C. M., & Brinkmann, J. 2006, *MNRAS*, 368, 715, doi: [10.1111/j.1365-2966.2006.10156.x](https://doi.org/10.1111/j.1365-2966.2006.10156.x)
- Mark, J. W. K. 1976, *ApJ*, 205, 363, doi: [10.1086/154287](https://doi.org/10.1086/154287)
- Mark, J. W. K. 1977, *ApJ*, 212, 645, doi: [10.1086/155087](https://doi.org/10.1086/155087)
- Masters, K. L., Krawczyk, C., Shamsi, S., et al. 2021, *MNRAS*, 507, 3923, doi: [10.1093/mnras/stab2282](https://doi.org/10.1093/mnras/stab2282)
- Michikoshi, S., & Kokubo, E. 2018, *MNRAS*, 481, 185, doi: [10.1093/mnras/sty2274](https://doi.org/10.1093/mnras/sty2274)
- Minniti, J. H., Zoccali, M., Rojas-Arriagada, A., et al. 2021, *A&A*, 654, A138, doi: [10.1051/0004-6361/202039512](https://doi.org/10.1051/0004-6361/202039512)
- Nair, P. B., & Abraham, R. G. 2010, *ApJS*, 186, 427, doi: [10.1088/0067-0049/186/2/427](https://doi.org/10.1088/0067-0049/186/2/427)
- Oh, S. H., Kim, W.-T., Lee, H. M., & Kim, J. 2008, *ApJ*, 683, 94, doi: [10.1086/588184](https://doi.org/10.1086/588184)
- Porter-Temple, R., Holwerda, B. W., Hopkins, A. M., et al. 2022, *MNRAS*, 515, 3875, doi: [10.1093/mnras/stac1936](https://doi.org/10.1093/mnras/stac1936)
- Sachdeva, S., Ho, L. C., Li, Y. A., & Shankar, F. 2020, *ApJ*, 899, 89, doi: [10.3847/1538-4357/aba82d](https://doi.org/10.3847/1538-4357/aba82d)
- Saha, K., & Elmegreen, B. 2016, *ApJL*, 826, L21, doi: [10.3847/2041-8205/826/2/L21](https://doi.org/10.3847/2041-8205/826/2/L21)
- . 2018, *ApJ*, 858, 24, doi: [10.3847/1538-4357/aabacd](https://doi.org/10.3847/1538-4357/aabacd)
- Salim, S., Boquien, M., & Lee, J. C. 2018, *ApJ*, 859, 11, doi: [10.3847/1538-4357/aabf3c](https://doi.org/10.3847/1538-4357/aabf3c)
- Salim, S., Lee, J. C., Janowiecki, S., et al. 2016, *ApJS*, 227, 2, doi: [10.3847/0067-0049/227/1/2](https://doi.org/10.3847/0067-0049/227/1/2)
- Salo, H., Laurikainen, E., Buta, R., & Knapen, J. H. 2010, *ApJL*, 715, L56, doi: [10.1088/2041-8205/715/1/L56](https://doi.org/10.1088/2041-8205/715/1/L56)
- Sanders, R. H., & Huntley, J. M. 1976, *ApJ*, 209, 53, doi: [10.1086/154692](https://doi.org/10.1086/154692)
- Sarkar, S., Narayanan, G., Banerjee, A., & Prakash, P. 2023, *MNRAS*, 518, 1022, doi: [10.1093/mnras/stac3096](https://doi.org/10.1093/mnras/stac3096)
- Savchenko, S., Marchuk, A., Mosenkov, A., & Grishunin, K. 2020, *MNRAS*, 493, 390, doi: [10.1093/mnras/staa258](https://doi.org/10.1093/mnras/staa258)
- Sellwood, J. A. 1985, *MNRAS*, 217, 127, doi: [10.1093/mnras/217.1.127](https://doi.org/10.1093/mnras/217.1.127)
- . 2000, *Ap&SS*, 272, 31, doi: [10.1023/A:1002668818252](https://doi.org/10.1023/A:1002668818252)
- . 2011, *MNRAS*, 410, 1637, doi: [10.1111/j.1365-2966.2010.17545.x](https://doi.org/10.1111/j.1365-2966.2010.17545.x)
- . 2012, *ApJ*, 751, 44, doi: [10.1088/0004-637X/751/1/44](https://doi.org/10.1088/0004-637X/751/1/44)

- Sellwood, J. A., & Carlberg, R. G. 1984, *ApJ*, 282, 61, doi: [10.1086/162176](https://doi.org/10.1086/162176)
- . 2023, *ApJ*, 958, 182, doi: [10.3847/1538-4357/acf9ee](https://doi.org/10.3847/1538-4357/acf9ee)
- Sellwood, J. A., & Masters, K. L. 2022, *ARA&A*, 60, doi: [10.1146/annurev-astro-052920-104505](https://doi.org/10.1146/annurev-astro-052920-104505)
- Sellwood, J. A., Shen, J., & Li, Z. 2019, *MNRAS*, 486, 4710, doi: [10.1093/mnras/stz1145](https://doi.org/10.1093/mnras/stz1145)
- Shu, F. H. 2016, *ARA&A*, 54, 667, doi: [10.1146/annurev-astro-081915-023426](https://doi.org/10.1146/annurev-astro-081915-023426)
- Smith, B. J., Giroux, M. L., & Struck, C. 2022a, *AJ*, 164, 146, doi: [10.3847/1538-3881/ac88c5](https://doi.org/10.3847/1538-3881/ac88c5)
- Smith, D., Habertzettl, L., Porter, L. E., et al. 2022b, *MNRAS*, 517, 4575, doi: [10.1093/mnras/stac2258](https://doi.org/10.1093/mnras/stac2258)
- Strateva, I., Ivezić, Ž., Knapp, G. R., et al. 2001, *AJ*, 122, 1861, doi: [10.1086/323301](https://doi.org/10.1086/323301)
- Struck, C. 2015, *MNRAS*, 450, 2217, doi: [10.1093/mnras/stv830](https://doi.org/10.1093/mnras/stv830)
- . 2024, *MNRAS*, 528, 7492, doi: [10.1093/mnras/stae485](https://doi.org/10.1093/mnras/stae485)
- Struck, C., Dobbs, C. L., & Hwang, J.-S. 2011, *MNRAS*, 414, 2498, doi: [10.1111/j.1365-2966.2011.18568.x](https://doi.org/10.1111/j.1365-2966.2011.18568.x)
- Toomre, A. 1969, *ApJ*, 158, 899, doi: [10.1086/150250](https://doi.org/10.1086/150250)
- Toomre, A. 1981, in *Structure and Evolution of Normal Galaxies*, ed. S. M. Fall & D. Lynden-Bell, 111–136
- Toomre, A., & Toomre, J. 1972, *ApJ*, 178, 623, doi: [10.1086/151823](https://doi.org/10.1086/151823)
- van den Bergh, S., Abraham, R. G., Ellis, R. S., et al. 1996, *AJ*, 112, 359, doi: [10.1086/118020](https://doi.org/10.1086/118020)
- Wake, D. A., Bundy, K., Diamond-Stanic, A. M., et al. 2017, *AJ*, 154, 86, doi: [10.3847/1538-3881/aa7ecc](https://doi.org/10.3847/1538-3881/aa7ecc)
- Willett, K. W., Lintott, C. J., Bamford, S. P., et al. 2013, *MNRAS*, 435, 2835, doi: [10.1093/mnras/stt1458](https://doi.org/10.1093/mnras/stt1458)
- Willett, K. W., Schawinski, K., Simmons, B. D., et al. 2015, *MNRAS*, 449, 820, doi: [10.1093/mnras/stv307](https://doi.org/10.1093/mnras/stv307)
- Xu, Y., Hao, C. J., Liu, D. J., et al. 2023, *ApJ*, 947, 54, doi: [10.3847/1538-4357/acc45c](https://doi.org/10.3847/1538-4357/acc45c)
- Yu, S.-Y., & Ho, L. C. 2020, *ApJ*, 900, 150, doi: [10.3847/1538-4357/abac5b](https://doi.org/10.3847/1538-4357/abac5b)
- Yu, S.-Y., Ho, L. C., Barth, A. J., & Li, Z.-Y. 2018, *ApJ*, 862, 13, doi: [10.3847/1538-4357/aacb25](https://doi.org/10.3847/1538-4357/aacb25)
- Zhang, Y.-C., & Yang, X.-H. 2019, *Research in Astronomy and Astrophysics*, 19, 006, doi: [10.1088/1674-4527/19/1/6](https://doi.org/10.1088/1674-4527/19/1/6)